

Disorder-Driven Pretransitional Tweed in Martensitic Transformations

Sivan Kartha

Institute for Advanced Study, Princeton, New Jersey 08540

James A. Krumhansl[†], James P. Sethna, and L. K. Wickham

*Laboratory of Atomic and Solid State Physics,
Cornell University, Ithaca, New York 14853-2501*

ABSTRACT: Defying the conventional wisdom regarding first-order transitions, *solid-solid displacive transformations* are often accompanied by pronounced pretransitional phenomena. Generally, these phenomena are indicative of some mesoscopic lattice deformation that “anticipates” the upcoming phase transition. Among these precursive effects is the observation of the so-called “tweed” pattern in transmission electron microscopy in a wide variety of materials. We have investigated the tweed deformation in a two dimensional model system, and found that it arises because the compositional disorder intrinsic to any alloy conspires with the natural geometric constraints of the lattice to produce a frustrated, glassy phase. The predicted phase diagram and glassy behavior have been verified by numerical simulations, and diffraction patterns of simulated systems are found to compare well with experimental data. Analytically comparing to alternative models of strain-disorder coupling, we show that the present model best accounts for experimental observations.

PACS numbers: 81.30.Kf, 75.10.Nr, 61.70.Wp

[†] Present Address:
Rd., Amherst, Massachusetts 01002

Introduction

Typically, first-order transformations occur abruptly. The liquid-vapor phase change, for example, is not heralded by critical fluctuations, length scales do not start diverging, and the system does not demonstrate large anticipatory excursions into the approaching phase. The textbook first-order behavior is fairly uneventful compared to universal critical phenomena associated with second-order transitions. In marked contrast to this well-established pattern, first-order *solid-solid* structural transformations (e.g. *martensitic* transformations) demonstrate pretransitional effects for as much as *hundreds* of degrees above the nominal transition temperature, despite their distinctly first-order nature. As witnessed in a wide-ranging variety of martensitic materials, this striking pretransitional behavior takes several different forms: anomalous phenomena in x-ray, electron, and neutron scattering including the quasi-elastic “central peak” observation in neutron scattering; partial elastic softening of various lattice distortive modes, including $q = 0$ homogeneous deformations as well as $q \neq 0$ phonon modes; anomalous behavior in transport coefficients and thermal expansion coefficients. One particularly distinctive example of such precursor phenomena is the observation of the “tweed” pattern (Figure 1) in transmission electron microscope images of materials approaching their martensitic transformation¹. In this paper we study tweed in materials undergoing martensitic transformations, with the aim of better understanding the origin and nature of pretransitional phenomena.

The main finding is that *disorder*, which is known to generally be important in these materials, may in fact play a fundamental role in bringing about pretransitional behavior, and that tweed can be generated as a direct response even to the simple statistical compositional disorder which is unavoidable in alloys. (Special defects are *not* required.) Further, we provide numerical evidence for the glassy behavior of tweed which earlier analysis had predicted². Our approach is 1) to introduce a model which exhibits a disorder-driven precursive tweed structure and to detail its phase diagram, 2) to analyze the simulated

x-ray diffraction data and real space images, and 3) to analytically compare this and other strain-disorder couplings by equating the disorder-induced long-range elastic forces with a non-local interaction in the order parameter, showing that the present model best accounts for experimental observations. The central importance of a disorder in any model which hopes to shed light on pretransitional phenomena is suggested by other experimental and computational studies as well, including the findings of Petry *et al.*³, who observe precursor effects in zirconium doped with small amounts of oxygen but not in pure zirconium, and Becquart *et al.*⁴, who observe tweed structures in molecular dynamics simulations of disordered materials but not ordered materials.

Background

Many materials of technological importance undergo martensitic transformations. In these solid-solid first-order structural transformations, the lattice deforms from one crystalline structure to another through some large-scale motion that preserves the topological integrity of the lattice, (i.e. there exists a “lattice correspondence.”) Unlike diffusive or order-disorder transformations requiring the interchange of atoms, these transformations are not *reconstructive*⁵, that is, bonds between neighbors are not broken and re-formed; there is no diffusion and atoms maintain their relationship with their neighbors. Rather, these transformations are *displacive*, meaning there is some homogeneous strain that transforms one lattice into the other, with atoms moving in a cooperative fashion, sometimes at sonic speeds. A simple example is the transformation of a square lattice into a rectangular lattice, brought about by stretching along one axis and shrinking along the other. Such transformations have sometimes been termed “military ” transformations, in order to convey the impression of a large-scale coordinated motion of an entire lattice, proceeding in lock-step from one configuration to another. This is in contrast to the relative anarchy of, say, a diffusive transformation, in which the atoms wander in search of a locally favorable environment, e.g. molecules in a vapor diffusing to find a home on a droplet.

The tweed pattern is seen as a pretransitional effect in transmission electron microscopy of many different materials, including shape memory alloys (NiAl⁶, FePd^{7,8,9}, CuAu¹⁰ etc.) and high temperature superconductors (A-15 compounds¹¹ V₃Si, Nb₃Sn, and the very high T_c YBaCuO-type^{12,13,14} and LaCuO-type cuprates etc), various other ceramics¹⁵ (e.g. Y₂O₃-ZrO₂), and alloys undergoing phase separation¹⁶ such as steel during tempering treatment¹⁷. As suggested by its name, the tweed pattern consists of diagonal striations bearing a striking resemblance to the tweed textile. The image has no strict periodicity, but there are two apparent length scales: one (call it L) corresponding to the longitudinal extent of the long diagonal striations and the other to their relatively short transverse width (ξ). These distances *appear* to be on the scale of tens or hundreds of lattice constants. However, it can be difficult to determine the lengthscales unambiguously, as artifacts of the imaging process can sometimes be confounded with genuine effects of the atomic configuration.

In order both to develop a formal theory and to test it by simulation, we consider as a model system a two dimensional solid which undergoes a structural phase transformation from a square lattice to a rectangular lattice as temperature is lowered^{18,19,20,21}. The two dimensional square \rightarrow rectangular transition corresponds to the tetragonal \rightarrow orthorhombic transition seen in planar compounds such as the YBaCuO-type and LaCuO-type high- T_c superconducting oxides. Conceptually, this is also the two dimensional analog of the cubic \rightarrow tetragonal transition seen in many materials, such as certain ferrous steels, shape memory alloys such as FePd and certain Indium alloys, and the superconducting A-15 compounds Nb₃Sn and V₃Si.

One very general and important experimental observation has attracted our attention to the role of disorder in these systems. Typically, alloys undergoing martensitic transformations are extremely sensitive to the relative alloying percentages of the elements which make them up. For example, Fe_{1- η} Pd _{η} undergoes its martensitic transformation at room

temperature when $\eta = 29\%$, but as η is increased to 32% , the transformation temperature, T_M , plummets to absolute zero: a one percent shift in the concentration of palladium causes a drastic $100^\circ K$ drop in T_M ! A convenient way to think of this drastic compositional sensitivity is to consider the martensitic transformation as a fixed temperature phase transition which occurs as η is varied and passes through some critical composition. The drastic dependence of transformation temperature on composition can then be viewed as simply a weak temperature dependence of the critical composition.

This drastic composition dependence of the transformation temperature is a commonly observed property of many of the martensitic materials that show pretransitional behavior. In our opinion, this striking property bears directly on the question of precursors and it offers some insight into their ubiquity. Since composition in any alloy or doped compound is a spatially inhomogeneous quantity, the *actual* composition will vary around some *average* composition simply due to the disorder that is frozen in as the solid crystallizes from the melt. Since the transformation temperature is so sensitive to composition, there must exist a locally defined hypothetical transformation temperature which depends on the local composition²². This local transformation temperature may be higher or lower than the observed transformation temperature, at which the first sign of bulk transformation is observed in a given sample, and long range martensitic order is actually established. For example, a small region in a sample of FdPd which has a lower than average concentration of palladium will seek to transform into the martensitic phase well before the transformation temperature at which the bulk martensitic order actually develops. The static, quenched-in, purely statistical compositional disorder will determine the spatial variation of local transformation temperature, and will thereby lead to pretransitional deformations occurring on a mesoscopic scale in a otherwise untransformed lattice.

In actuality any local tendency to transform may be suppressed by the surroundings which may not be ready to transform. Therefore, the essence of this problem is to treat

the overall system as a collection of local regions which *interact* via extended strain fields. It cannot be a simple superposition of different transformable units, nor can models which simply address isolated defects produce the pretransitional effects we propose. Cooperative behavior, we believe, is of the essence.

Theory and Model

We seek here to model this coupling between compositional disorder and the martensitic transformation, and to understand the nature of the lattice deformation which arises in response. Since the tweed structure we are investigating is a lattice deformation with a length scale of many lattice constants, we will adopt a perspective which focuses on this mesoscale structure, and leaves the atomistic behavior of the material largely unspecified. To this end, we will view the material as an elastic continuum, and analyze it within a Landau-Ginzburg framework governing the lattice distortive free energy. Pursuing this approach, we construct a general free energy which is consistent with the symmetries of the system and which is taken to sufficiently high order in the relevant strain order parameters to produce the important physical behavior. The parameters in the resulting free energy are related to empirically measurable materials constants, such as elastic constants, phonon dispersion curves, couplings to impurities, lattice constants etc.

At the outset, we emphasize that the fundamental cause of tweed in our theory is simply local (static) variations in the effective coarse grained free energy arising from compositional variation. While models which also couple to reconstructive ordering, or other chemical reactions, have yielded tweed in simulations^{18,19}, we suggest that ordering, *per se*, is not a fundamental cause of tweed. No ordering or reconstruction of any kind takes place in the tweed and martensite regimes of almost any of the well known alloys or ceramics that show this precursor behavior. Perhaps, in fact, it is best to think of ordering or other replacive effects simply as additional ways, beyond composition, to produce spatial variation in the coarse grained free energy of our model. Again, then, it is the cooperative

elastic behavior of regions of locally different coarse grained free energy which we propose to be the generic origin of this kind of precursor.

The two dimensional system is modeled by the following free energy relative to a perfect square reference lattice:

$$f = \frac{A_1}{2}e_1^2 + \frac{A_2}{2}e_2^2 + \frac{A_\phi}{2}\phi^2 - \frac{\beta}{4}\phi^4 + \frac{\gamma}{6}\phi^6 + \frac{\kappa}{2}(\nabla\phi)^2 \quad (1)$$

which is a functional of the strain fields $e_1(x, y)$, $e_2(x, y)$, and $\phi(x, y)$. Here, $e_1 \equiv (e_{xx} + e_{yy})/\sqrt{2}$ is the bulk dilational strain; $e_2 \equiv e_{xy}$ is the shear strain; and $\phi \equiv (e_{xx} - e_{yy})/\sqrt{2}$ is the deviatoric (or rectangular) strain²³. The symmetric strain tensor \mathbf{e} is defined in the standard way²⁴ as the non-rotational part of the displacement gradients,

$$e_{ij} \equiv \frac{1}{2}\left(\frac{\partial U_i}{\partial x_j} + \frac{\partial U_j}{\partial x_i} + \frac{\partial U_l}{\partial x_i}\frac{\partial U_l}{\partial x_j}\right). \quad (2)$$

The second order term guarantees that finite rotations are not included in the strain tensor, but in general this term is very small for these applications, and we have safely neglected it in our analytical work, although all numerical simulations include it.

The first three terms in the free energy (1) simply mean that the material in question has a Hooke's law restoring force to deformations into the dilational, shear, and rectangular strain modes. (These, of course, are the only three homogeneous elastic modes available to a two dimensional solid with square symmetry.) The coefficients in front of those three terms are simply the harmonic elastic constants of the material, where $A_1 = C_{11} + C_{12}$, $A_2 = 4C_{44}$, and $A_\phi = C_{11} - C_{12} = 2C'$. The free energy also includes higher order (i.e. anharmonic) terms in the rectangular strain, ϕ , in order to produce a first-order phase transition from a square "austenite" phase with $\phi = 0$ to a rectangular "martensite" phase with $\phi = \pm\phi_M$. This phase transition occurs as the elastic constant A_ϕ "softens", (i.e. decreases with temperature), and below a (nonzero!) critical value $A_\phi^{crit} = \frac{3\beta^2}{16\gamma}$ the rectangular phase becomes the stable phase, with the transformation strain $\phi_M =$

$((\beta + \sqrt{\beta^2 - 4A_\phi\gamma})/2\gamma)^{\frac{1}{2}}$. The parameters β and γ are determined by the magnitude and the energy of the martensitic strain at the critical temperature²⁵

We introduce compositional disorder in the simplest way which is consistent with the symmetries of the problem. The elastic constant A_ϕ is allowed to be not only temperature dependent, but also composition dependent. The dependence of A_ϕ on both temperature and composition is taken to be a simple linear relationship, thereby quadratically coupling the strain order parameter ϕ to the random composition field:

$$A_\phi(\mathbf{x}) = A_T \cdot (T - T_0(\bar{\eta})) + A_\eta \cdot \delta\eta(\mathbf{x}) \equiv \bar{A}_\phi + \delta A_\phi. \quad (3)$$

Here, $T_0(\bar{\eta})$ is the temperature marking the mechanical instability of the austenite phase at the nominal composition $\bar{\eta}$, and A_T and A_η describe the linear dependence of the elastic constant A_ϕ on temperature and composition, respectively. The spatially varying (but temporally constant) field $\delta\eta(\mathbf{x}) \equiv \eta(\mathbf{x}) - \bar{\eta}$ is the local deviation from the average composition. Its value on each simulation cell is determined by selecting a random value from a gaussian distribution of unit width. (By normalizing to unit width, the *magnitude* of compositional inhomogeneity and the *strength* of its coupling to the elastic constant A_ϕ are both included in the coupling parameter A_η .) Then, the local “transformation temperature” is given by $T_M(\mathbf{x}) = T_M(\bar{\eta}) - \frac{A_\eta}{A_T} \cdot \delta\eta(\mathbf{x})$.

At high temperatures, all the regions of the system will prefer to be in the undeformed phase, and at low temperatures all will prefer the martensitic phase. However, near the bulk transformation temperature, there will be a temperature range given by the typical magnitude of $\frac{A_\eta}{A_T} \cdot \delta\eta(\mathbf{x})$, where the coupling between the strain ϕ and the random compositional disorder can provide a non-negligible driving force toward a pretransitional deformation. Using numerical simulations and analysis, we shall show that a pretransitional deformation does occur for the present model, and that it is tweed.

Simulation

Figure 2 displays the results of a computer simulation of the model described above. Configurations 2(a-e) show the development from the undeformed austenite phase, through a pretransitional regime, into the fully developed martensite phase, as the elastic constant A_ϕ softens. One immediately recognizes the telltale diagonal modulations of tweed developing in the pretransitional regime. The simulation reveals that the system does indeed accomodate the energetic demands of the compositional disorder by generating a deformation as shown, i.e. the tweed modulation is the natural response of the system to the disorder.

The configurations in Figure 2 are generated by simulating the continuum system described above, discretized onto a 51×51 mesh. The simulation variables are the displacements U_x and U_y at each site, and using a finite difference scheme the strains and strain gradients are found for use in calculating the free energy (1). A random composition field which varies around some average concentration $\bar{\eta}$ is assigned at the beginning and held static. The full rotationally invariant strain tensor is calculated from any arbitrary displacement field, and then used to find the total energy of the system. A Monte Carlo simulated annealing algorithm is used to minimize this energy, and generate a stable low energy configuration for a given point in parameter space. Typically, we quench over four decades of temperature, using three thousand Monte Carlo steps per lattice site per decade.

The materials parameters used in the simulation are those appropriate for FePd. Static harmonic elastic constant measurements⁹ have given us A_ϕ ($2.5 \cdot 10^{10}$ N/m² at the onset of tweed), A_2 ($28 \cdot 10^{10}$ N/m²), and A_1 ($14 \cdot 10^{10}$ N/m²). The strain gradient parameter κ/a^2 ($2.5 \cdot 10^{10}$ N/m²) can be calculated from the curvature of the TA₁ phonon dispersion curve²⁶. The coefficients β (1.710^{13} N/m²) and γ ($3 \cdot 10^{16}$ N/m²) are determined by the martensitic strain and the value of A_ϕ at the transition. The coupling to temperature, A_T ($2.4 \cdot 10^8$ N/m² K), is known from measurements⁹ of the temperature dependence of A_ϕ . The coupling to statistical compositional variations, A_η , will be discussed in detail

below.

A phase diagram, Figure 3, generated by the simulation, is straightforward and intuitively sensible. The vertical axis is the elastic constant \bar{A}_ϕ at the nominal composition, i.e. the “average” value of the elastic constant. Since \bar{A}_ϕ softens linearly with temperature over a large temperature range (at least $150^\circ K$), this axis also effectively reflects temperature. The horizontal axis²⁷ is the strength of the coupling, A_η , between the strain order parameter ϕ and the composition inhomogeneity, $\delta\eta$. The general structure of the phase diagram is good confirmation of the general mechanism underlying our model: sufficiently far from the thermodynamic transformation temperature for the nominal composition, the expected conventional phases appear, while near to the transformation temperature there is a region where the effect of the disorder becomes important, the lattice deforms, and tweed appears.

In experimental observations⁷, as the temperature of a sample is lowered toward the martensitic transformation temperature, a smooth and unremarkable TEM image gives way to a mottled pattern which signals the onset of some static lattice distortion — static at least on the time-scale of TEM observations. With further decrease in temperature, the mottled pattern organizes into a pattern with a distinguishable directionality, acquiring a noticeable but diffuse tweediness. As the transformation temperature is approached, the tweed develops increasingly coarse and long-range correlations, and as the sample passes through the martensitic transformation, the tweed gives way to fully transformed martensite, perhaps nucleating the emerging finely twinned structure²⁸.

In direct correspondence with these experimental observations, the simulation yields precisely this same progression of pattern development as \bar{A}_ϕ is decreased, (where A_η is held fixed at some constant value). A perfectly undeformed system is initially interrupted by scattered, non-interacting and uncorrelated regions of distortion. These are regions which have relatively large values of $\delta\eta$ (large negative values, since A_η is positive for

FePd) and are therefore the first to transform from the (locally metastable or eventually unstable) austenite phase. Within the constraints of the surrounding lattice, they thus deform precociously toward the martensitic phase, giving the system a mottled appearance. (This is the region above the austenite-tweed boundary.) As \bar{A}_ϕ is further lowered, these regions grow dense enough to interact, and longer range diagonal correlations develop, yielding a diffuse tweed which grows increasingly distinct as \bar{A}_ϕ is further lowered. As \bar{A}_ϕ approaches the nominal transformation temperature of the sample, an increasing fraction of the sample prefers the martensitic phase, and the tweed grows very coarse before finally transforming into the twinned martensite configuration (which lies below the tweed–martensite boundary.) The precise placement of the austenite–tweed boundary is somewhat ill-defined, as the distinction between “correlated” and “uncorrelated” is subjective, particularly in small samples such as those studied here. (A quantitative study of the degree of correlation can be found elsewhere²⁹.) The tweed–martensite boundary, however, is well-defined, as the onset of long–range martensitic order is a qualitative transition that can be located precisely.

The parameters in this phase diagram are \bar{A}_ϕ (or equivalently, temperature) and the strength of the coupling to compositional variations, A_η . In the laboratory, temperature is easily varied, but for any given alloy the coupling strength is an unadjustable property of the material, so the behavior of a sample will trace a trajectory through the phase diagram which falls along a single line, presumably with essentially constant A_η . (Alternately, holding temperature fixed, the behavior of a material may be investigated over a range of \bar{A}_ϕ by studying samples of varying nominal compositions, $\bar{\eta}$.) By comparing the electron microscopy observations of FePd to the phase diagram derived from simulations, we determine the effective value of A_η . In experimental investigations of FePd⁹ the onset of tweed is seen to be roughly one hundred degrees above the transformation temperature, corresponding to $A_\phi = 2.5 \cdot 10^{10} \frac{N}{m^2}$. By matching to the experimentally observed tweed

range, we determined the strength of the coupling to composition variation required to generate tweed over this range in our simulation; the value found is $A_\eta \approx 2.0 \cdot 10^{10} \frac{N}{m^2}$. This figure may be compared to the following somewhat simplistic estimate for A_η . If, say in a binary alloy such as FePd, the full “bulk” composition variation ($d\bar{A}_\phi/d\bar{\eta}$) coefficient were assigned to each lattice site, and the composition at each simulation site varied between pure Fe or Pd, the statistical fluctuation of A_ϕ would be 50 times larger than that found to be required in our simulations. This result should be regarded in the light that there is apparently plenty of driving force provided by simple compositional variations to produce tweed, even in the absence of any specific defects or order–disorder changes.

This rather large estimate for the coupling A_η neglects several important points which should be considered in any careful attempt to calculate the coupling to composition:

- 1) $d\bar{A}_\phi/d\bar{\eta}$ is the product of $dT_M/d\bar{\eta}$ and dA_ϕ/dT , where each of these are known from experimental measurements near T_M . Linearly extrapolating away from the range of $\bar{\eta}$ (29% to 32%) over which the martensitic transformation occurs may well overestimate its strength for concentrations outside of this range. As mentioned above, it is convenient to think of the martensitic transformation as occurring at a (weakly temperature dependent) critical composition, so it is perhaps more accurate to consider $A_\phi(\bar{\eta})$ as a step function at the critical composition, say, rather than a simple linear function.
- 2) As will be discussed further below, finite temperature effects are important in these systems. Thermal lattice vibrations are quite substantial at the temperatures at which tweed is seen, and will be correlated over some temperature dependent length scale, transmitting and averaging out the effects of any disorder, including local compositional variation.
- 3) In any Landau–Ginzburg theory of a non-uniform system, the existence of a local free energy, (a concept which is thermodynamic in nature,) implicitly assumes that one has “integrated out” certain (secondary) degrees of freedom. For example, defining a free energy functional of a static strain tensor requires integrating over phonon modes, which necessarily introduces a

coarse-graining length scale^{30,31}. Introducing this length scale into the problem will result in averaging the effect of compositional variations (and will also change other parameters of the model). 4) Any physical mechanism which is based on the chemistry of an alloy or doped compound will involve electronic effects which will exert their influence over a length scale which is larger than the lattice spacing, typically on the order of a Fermi length. Again, this will lead to a spatial averaging of composition, weakening the apparent strength of the coupling to local compositional variation. 5) This two dimensional model, although faithful to the real three dimensional material from the perspective of symmetry requirements, neglects an important effect of dimension on compositional fluctuation: a composition field which is defined by averaging within some radius will average over a region of material which whose size will depend on dimension. Correspondingly, in a higher dimension there will be smaller compositional fluctuations.

Spin Glass and Tweed

The dotted lines in the phase diagram (Figure 3) are drawn to provide a comparison between the model presented here and earlier work² in which the martensitic system was treated analytically by taking the approximation of infinite elastic anisotropy³² and formally mapping tweed onto a spin glass system. The infinite anisotropy approximation is motivated by the observation of severe softness of A_ϕ in many martensitic materials, and a corresponding growth of the elastic anisotropy, $\alpha \equiv C_{44}/C'$. (For example, in FePd $\alpha \sim 20$, in NiAl $\alpha \sim 10$, and in some Indium alloys α approaches ~ 300 !³³.) As discussed fully below, solutions in this approximation are given by displacement fields of the form

$$\mathbf{U}(x, y) = \begin{pmatrix} 1 \\ -1 \end{pmatrix} U_+(x + y) + \begin{pmatrix} 1 \\ 1 \end{pmatrix} U_-(x - y) \quad (4)$$

where U_+ and U_- are arbitrary functions of position along the $\langle 11 \rangle$ and $\langle 1\bar{1} \rangle$ directions. These limiting solutions clearly have infinitely long correlations in the diagonal directions, explaining why there is natural tendency for a tweed-like, diagonal modulation. (This

tendency for a displacement field is related to the fact that twin boundaries appear only along $\langle 11 \rangle$ directions.) Although this is clearly a very severe constraint on the form of the allowed solutions, such displacement fields are surprisingly still capable of smoothly and continuously modulating between regions of the high and low temperature phases. That is to say, regions of the austenite and the two martensitic variants can be patched together without generating any of the two energetically costly strains, e_1 and e_2 . As in the full elastic model of this paper, it is compositional inhomogeneities which generate a local propensity toward one phase or the other, and thereby provide the driving force behind the tweedy modulation.

The approximation of infinite elastic anisotropy helps to explain how the lattice manages to accomodate the compositional disorder, but further, it demonstrates the subtlety of that accomodation. In the effort to adjust to the local disorder, subject to the constraint of infinite diagonal correlations, the displacement field suffers substantial frustration. As in many systems, this coupling of disorder (compositional) and frustration (elastic strain) gives rise to glassy behavior. In a formal and rigorous way, this claim can be made mathematically precise, and the martensitic system can be mapped to an infinite range bipartite Sherrington–Kirkpatrick spin glass. (See Ref. 2 for details.) Tweed is therefore an intermediate phase between the high temperature square phase and the low temperature rectangular phase, in direct correspondance with the spin glass phase which exists between the ferromagnetic and antiferromagnetic phases.

Admittedly, actual materials do not have *infinite* elastic anisotropy: one should therefore not too boldly assert claims founded on what amounts here to a mean–field approximation. Tweed, which in this approximation is an actual thermodynamic phase with second order phase boundaries, will appear in the real world as a “ghost” of an intermediate phase, perhaps without true long-range order in time, but with observable glassy behavior. It is therefore of particular interest to investigate the nature of the remaining glassy behavior

when we relax the approximation of infinite elastic anisotropy.

The numerical simulation, which uses materials parameters appropriate for FePd, allows us to gain insight into the nature of the glassy manifestations in a system with realistic finite elastic anisotropy. In particular, we can observe the transition to glassy behavior in our numerical simulation as temperature is decreased. Note, as explained above, temperature is introduced into the simulation through the temperature dependence of the softening elastic constant A_ϕ . However, the Monte Carlo method we have adopted allows us to also introduce thermal fluctuations and study their ability (or inability, as the case may be) to destroy the long range order in time which is the signature of a glassy system. Using the number of attempted Monte Carlo steps per site (MCS) as a measure of time, we have identified a regime in phase space where fluctuations become very slow.

To quantify such glassy behavior, we have measured time correlations of the martensitic ϕ distortion. Because this strain fluctuates around a zero mean, the quantity³⁴:

$$\xi(t) \equiv \frac{1}{N} \sum_i \phi(\text{site } i, \text{time } 0) \phi(\text{site } i, \text{time } t)$$

will be zero unless the values of ϕ at time zero and time t are correlated. Figure 4 shows values for this correlation function, after normalizing to $\xi(0) = 1$ and averaging over a number of intervals for each time t for improved statistics. All of the data in the graph were produced with a single set of parameters which gave clear tweed when thermal fluctuations were negligible. The physical temperature given for each curve is determined from the Monte Carlo temperature by using the known elastic constants, strains, and the appropriate grid spacing to equate the Monte Carlo fluctuations with a thermal Boltzmann distribution.

The behavior at the two temperatures differ sharply. At 38 K, memory of the deformations present at $t=0$ lasts over tens of thousands of steps, as some local distortions have been unable to surmount the potential barrier between one martensitic variant and

the other. At 380 K, however, all areas in the lattice are able to fluctuate between both martensitic variants, and memory of the original configuration is nearly lost after merely a hundred MCS. Using a typical frequency for atomic motion and the size of each Monte Carlo step (which was held constant in this part of the study), we can estimate that a thousand Monte Carlo steps corresponds to several picoseconds. Since the time scale for neutron scattering is of order picoseconds, we emphasize that there exists a regime in the numerical simulations for which the resulting deformations constitute a robust tweed pattern which is static for a duration which is experimentally significant.

Clearly, the low temperature model in Figure 4 has a wide distribution of relaxation times, characteristic of glassy behavior. If our system were a true spin glass on an infinite lattice, the longest relaxation time scales would diverge and there would be true long range order in time³⁵. Experimental observations of physical systems which display spin glass behavior have observed relaxation times of days or weeks³⁵. Even spin glass simulations on small lattices have relaxation spectra which are bounded above only by the (rather large) time scale associated with flipping all of the spins in the lattice. To get a grasp of how long such waiting times might be in our system, recall that the mapping from a spin glass to our infinite anisotropy model maps one spin to a correlated region as long as a lattice diagonal, so that the energy to flip over a “cluster” of our “spins” is really the overwhelming elastic energy barrier to reversing strain in several long, overlapping tweed strips. In our finite anisotropy limit, correlated tweed regions are still large compared to the lattice constant, so the dynamics in our model will still resemble that expected in a (large but finite) spin glass³⁶. It seems likely that the hysteresis⁸ and frequency dependent relaxation³⁷ seen in the tweed regime in real materials hints at the glassy, slow dynamics predicted by our model.

Diffraction

Transmission electron microscopy studies are not always designed to yield direct infor-

mation about the underlying atomic displacements. It is therefore useful to refer to the diffraction images produced in conjunction with the tweed observations. Figure 5a shows experimental¹⁴ x-ray diffraction contours taken from tweed produced in YBaCuO, and Figure 5b shows diffraction patterns at the same Bragg peaks for the simulated tweed computed directly by Fourier transforming the displacements in the simulation. As can be seen, the qualitative features are faithfully reproduced.

Beyond the simple reassurance derived from qualitatively matching simulated diffraction patterns with experimental results, additional information comes from focusing on reciprocal space since real space strain images and reciprocal space diffraction patterns yield different information under the time averaging present in any data collection process. In a real space image which makes one martensitic variant light and another dark, a region which is fluctuating quickly from one variant to the other would appear to be grey in a coherent time average. (This could be the case for a tetragonal to orthorhombic transformation observed under “two-beam” TEM imaging, which shows strain projected along a given direction.) In a diffraction pattern from sample of tweed, the characteristic cross pattern is a result of *correlations* in strain, not just the *absolute* strain. Even if the specific martensitic deformations vary in time, the incoherent time average which is given in a diffraction pattern will still show clear streaks as long as the strains maintain persistent instantaneous correlations.

Figure 6 demonstrates that “static” tweed (upper row) melts to a “dynamic” tweed (lower row) as temperature is increased³⁸. The first column shows the instantaneous configuration: the distinctly tweedy deformation in the upper sample is largely obscured in the lower sample by thermal fluctuations. The middle column shows an average of real-space deformations over 150,000 attempted Monte Carlo steps (corresponding to averaging over approximately a nanosecond). The tweed in the upper sample is still easily discerned, whereas the lower sample has averaged to virtually zero net deformation. However, both

simulated samples yield a time-averaged diffraction pattern with the characteristic diagonal streaking, revealing the presence of instantaneous tweedy correlations. This is analogous to the presentation of Van Tendeloo *et al.*³⁹, who show that the tweedy correlations of static and dynamic tweed can be verified by their diffraction images, even though they behave very differently over the relatively long time required to make a TEM image.

Of course, “static” and “dynamic” are only defined on the time scale of the relevant real space observations. However, our theory predicts a clear transition to macroscopically long range order in time, and current evidence supports this prediction. Molecular dynamics simulations of tweed in NiAl have found a change from static to dynamic behavior with increased temperature⁴, and neutron diffraction and TEM observations of real NiAl find a static component of tweed which appears and then grows as the temperature is lowered⁴⁰. In our own numerical simulations, we’ve observed such a transition by detecting the onset of correlations below some temperature. For example, the static tweed of Figure 6 is static (on a time scale of several thousands MCS) from 0K to roughly 70K, and dynamic from 70 K to 90 K. Similarly, the dynamic tweed of Figure 6 actually arises from a sample which is fully twinned up to roughly 76K, and then is a dimly visible (i.e. static⁴¹) tweed at 85K, and then is dynamic at temperatures as high as 114K. Quantitatively, this same transition is demonstrated in Figure 4.

Thus, in our model, both static and dynamic tweed are present over temperature ranges of tens of degrees Kelvin. In a real three dimensional sample, one can assume there would be an even larger tweed range, since thermal fluctuations are more heavily damped in three dimensions. The simulation results also serve as a reminder that, depending on the material in question, either “static” or “dynamic” behavior may dominate most of the temperature range of tweed. Since available experimental probes react differently to changes in dynamical behavior, understanding variations in the time dependence of tweed will be vital for appropriate comparison of data. These concerns apply not only to

diffraction patterns and TEM images, but also to the “central peak” of inelastic neutron scattering, which has been associated with tweed which is static on the time scale of neutron scattering⁴⁰. Interestingly, our findings also indicate that introducing thermal fluctuations can produce a transition from martensite to tweed, once again implicating the long suspected influence of vibrational entropy as a stabilizing effect for the high temperature phase.

It has long been known¹⁶ that the diffraction patterns such as those shown above are consistent with the presence of $\{110\}$ planes shearing in $\langle 1\bar{1}0 \rangle$ directions, the so-called Zener mode⁴². The square \rightarrow rectangular transformation considered here, as well as the cubic \rightarrow tetragonal and tetragonal \rightarrow orthorhombic transformations all result from precisely such $\{110\}/\langle 1\bar{1}0 \rangle$ shears. In addition, this shear (coupled with an additional homogeneous strain) is responsible for body-centered cubic \rightarrow close-packed transformations. The observation of a pretransitional deformation which involves this particular shear is therefore very consistent with the approach of the martensitic transformation. Furthermore, it is this shear mode that couples to the elastic constant A_ϕ which is seen to soften in many materials as the martensitic transformation temperature is approached and which motivated the approximation of infinite elastic anisotropy discussed above.

For completeness, let us make explicit the connection between the observed diffraction behavior and the lattice displacements. To consider the diffraction pattern from a distorted lattice, we make use of the fact that an arbitrary displacement field can be written in a perfectly general way as

$$\mathbf{U}(x, y) = \begin{pmatrix} 1 \\ -1 \end{pmatrix} U_+ \left(\frac{x+y}{d}, \frac{x-y}{L} \right) + \begin{pmatrix} 1 \\ 1 \end{pmatrix} U_- \left(\frac{x+y}{L}, \frac{x-y}{d} \right). \quad (5)$$

In the infinite anisotropy approximation, L would be taken to be infinity, yielding eq.(4). A displacement consisting of long (but not infinite) diagonal correlations can be expressed by taking $L \gg d$ (where we define U_- and U_+ such that they have similar functional

dependences on their first and second arguments.) The correlation length L then describes the longitudinal length scale of the tweed striations, and d describes their transverse width.

The general expression⁴³ for the diffracted intensity at a wavevector \mathbf{Q} , (scattering from sites \mathbf{s} with structure factors $f_{\mathbf{s}}$) is

$$I(\mathbf{Q}) = \left| \sum_{\mathbf{s}} f_{\mathbf{s}}(\mathbf{Q}) e^{i\mathbf{Q} \cdot \mathbf{R}_{\mathbf{s}}} \right|^2. \quad (6)$$

If we write $\mathbf{Q} = \mathbf{K} + \mathbf{q}$ (where \mathbf{K} is the nearest reciprocal lattice vector to \mathbf{Q}) and write $\mathbf{R}_{\mathbf{s}} = \mathbf{R}_{\mathbf{s}}^{\circ} + \mathbf{U}_{\mathbf{s}}$ (where $\mathbf{U}_{\mathbf{s}}$ is a displacement around the lattice point $\mathbf{R}_{\mathbf{s}}^{\circ}$) then we can expand (6) assuming small displacements and find:

$$I(\mathbf{Q}) = |f(\mathbf{Q})|^2 \left| \sum_{\mathbf{s}} (\mathbf{Q} \cdot \mathbf{U}_{\mathbf{s}}) e^{i\mathbf{q} \cdot \mathbf{R}_{\mathbf{s}}^{\circ}} \right|^2$$

(where for convenience we have assumed a monotomic lattice, or at least a lattice with an effectively constant $f_{\mathbf{s}}$). Fourier expanding $\mathbf{U}_{\mathbf{s}}$ and noting that the summation over sites will give us a delta function, we find:

$$I(\mathbf{Q}) = |f(\mathbf{Q})|^2 |\mathbf{Q} \cdot \mathbf{U}_{\mathbf{q}}|^2. \quad (7)$$

Eq.(7) indicates that, in the approximation of small displacements, the intensity of diffuse scattering around Bragg peaks (normalized by $1/|f(\mathbf{Q})|^2$ will obey a $|\mathbf{Q}|^2$ dependence. Comparing the observed scattering intensity to a $|\mathbf{Q}|^2$ fit will allow us to verify that the scattering is caused by a *small* lattice deformation. Substantial deviation from a strict $|\mathbf{Q}|^2$ dependence would imply that the approximation of scattering from small displacements is not appropriate, suggesting that the scattering is due perhaps to substitutional disorder or to microdomains large enough to produce size broadening¹⁴. Figure 7 shows the diffuse scattering intensity (normalized by the appropriate structure factor) plotted for Bragg peaks $\langle 0 \ Q \ 0 \rangle$, with $Q/(2\pi/a) = 4, 6, 8$, and 10 for the experimental measurements¹⁴ (filled circles) and $Q/(2\pi/a) = 0, 1, 2, \dots, 10$ for our simulated diffraction patterns (open circles).

The curve shows the best $|\mathbf{Q}|^2$ fit to the experimental data. The minor deviation from the $|\mathbf{Q}|^2$ fit reflects the fact that displacements are finite, yet small.

Assured that we are indeed observing diffuse scattering from small displacements, we can proceed by solving the Fourier transform of eq.(5), $\tilde{\mathbf{U}}(\mathbf{k}) = \tilde{\mathbf{U}}_+(\mathbf{k}) + \tilde{\mathbf{U}}_-(\mathbf{k})$, where

$$\tilde{\mathbf{U}}_+(\mathbf{k}) = \int \frac{dxdy}{\sqrt{A}} \begin{pmatrix} 1 \\ -1 \end{pmatrix} U_+(\frac{x+y}{d}, \frac{x-y}{L}) e^{i \mathbf{k} \cdot (\mathbf{x}+\mathbf{y})} \quad (8a)$$

$$\tilde{\mathbf{U}}_-(\mathbf{k}) = \int \frac{dxdy}{\sqrt{A}} \begin{pmatrix} 1 \\ 1 \end{pmatrix} U_-(\frac{x+y}{L}, \frac{x-y}{d}) e^{i \mathbf{k} \cdot (\mathbf{x}+\mathbf{y})} \quad (8b)$$

Make the substitutions $k_{\pm} \equiv (k_x \pm k_y)/\sqrt{2}$ and

$$s \equiv \frac{(x+y)}{d\sqrt{2}}, \quad \text{and} \quad t \equiv \frac{(x-y)}{L\sqrt{2}}$$

in eq. (8a) and

$$s \equiv \frac{(x+y)}{L\sqrt{2}}, \quad \text{and} \quad t \equiv \frac{(x-y)}{d\sqrt{2}}$$

in eq. (8b). We then find

$$\tilde{\mathbf{U}}_+(\mathbf{k}) = \frac{Ld}{\sqrt{A}} \int dsdt \begin{pmatrix} 1 \\ -1 \end{pmatrix} U_+(s, t) e^{i (dk_+s + Lk_-t)} \quad (9a)$$

$$\tilde{\mathbf{U}}_-(\mathbf{k}) = \frac{Ld}{\sqrt{A}} \int dsdt \begin{pmatrix} 1 \\ 1 \end{pmatrix} U_-(s, t) e^{i (Lk_+s + dk_-t)} \quad (9b)$$

The general shape of this Fourier transform is clear by inspection: expression (9a) is simply a Fourier transform of $U_+(s, t)$ *scaled* by $1/d$ along the $\hat{\mathbf{s}}$ direction and $1/L$ along the $\hat{\mathbf{t}}$ direction (similarly for U_-). Since, by construction, U_+ and U_- are simple isotropic displacement fields, then so are their Fourier transforms, and the final result is a Fourier transform, $\tilde{\mathbf{U}}(\mathbf{k})$ which has the shape of two diagonal streaks emanating from the origin, the length of each streak being $\sim 1/d$, and the width $\sim 1/L$. In addition to the variation in diffuse scattering with $|\mathbf{Q}|$ discussed earlier, there is also a marked variation with the orientation of \mathbf{Q} , as demonstrated in Figure 5. The product $\mathbf{Q} \cdot \mathbf{U}_{\mathbf{q}}$ in Eq.(7) will cause diffuse scattering resulting from U_+ to vanish for $\mathbf{Q} \parallel (1, 1)$ and the diffuse scattering from

U_- to vanish for $\mathbf{Q} \parallel (1, -1)$. This is known as the “extinction condition” associated with $\{110\}/\langle 1\bar{1}0 \rangle$ shears. (Ref. 29 discusses extracting d and L from data.)

Figure 8 shows the trace of the diffuse scattering around the Bragg peak (660) in the $\langle \bar{1}10 \rangle$ direction for YBaCu(Al)O. The corresponding simulation diffraction data is also shown, averaged over several simulation runs for improved statistics and scaled by a single constant for both the $\langle \bar{1}10 \rangle$ direction and the $\langle 110 \rangle$ direction. The simulation data points closely follow experimental points for the regime covering the first two orders of magnitude of intensity, but then fall off quickly, partly due to the absence in the simulated diffraction pattern of background scattering which is experimentally unavoidable. As Jiang *et al.* have shown¹⁴ for YBaCu(Al)O, the $1/q^2$ behavior indicated by the line corresponds to a lattice distortion which can be explained as a linear elastic response in a material with a random distribution of oxygen atoms. The fact that the intensity falls off quicker than $1/q^2$ is offered by them as evidence for non-random short range (~ 40 Å) correlation in the oxygen ordering. We attach no great significance to the agreement between experiment and our simulations: our theory is non-linear, but far from the transformed regions (small q) the strain field is dominated by linear response. It is simply reassuring that the computed structure of the scattering profile is consistent with experiment.

Compatibility and Nonlocal Interactions

Having reviewed the explicit relationship between the tweed deformation and the observed diffraction pattern, we wish now to explain the physics underlying that deformation. We wish to repeatedly emphasize that an essential aspect of the physics underlying tweed is that any local fluctuation in the elastic free energy functional (e.g., due to compositional inhomogeneity) cannot be regarded in isolation. The lattice response is not simply a superposition of the responses expected for independently considered sites of disorder. Rather, mutual non-local interactions between spatially separated regions conspire to give

an extended cooperative response: i.e. the tweed phenomenon. In this section, we here develop a simple yet illuminating analysis which explicitly uncovers the effective non-local interaction which leads to these extended cooperative responses. We write the non-local interaction in terms of a renormalized Fourier space elastic constant, and show that the specific form of the tweed deformation immediately follows.

The only explicitly non-local term in the free energy Eq. (1) is the strain gradient term $(\nabla\phi)^2$. However, even disregarding this term, the order parameter ϕ cannot be an entirely arbitrary function of position: there is no guarantee that such a field (even if continuous) is physical. This problem relates to the following important subtlety of any Landau-Ginzburg-type model which treats elastic strain as the relevant order parameter: the true degrees of freedom in a continuum elastic medium are contained in the *displacement* field, $\mathbf{U}(\mathbf{x})$, even though it is the *strain* fields, e_{ij} , which appear in the free energy. Instead of treating the strains as independent fields, one must assure that they correspond to a physical displacement field, i.e. that they are derivatives of a single continuous function. This is done by requiring that they satisfy a set of non-trivial *compatibility relations*⁴⁴ concisely expressed by the equation⁴⁵ $\nabla \times (\nabla \times \mathbf{e})^\dagger = \mathbf{0}$. In two dimensions this can be written as

$$\nabla^2 e_1 - \sqrt{8} \partial_{xy} e_2 - (\partial_{xx} - \partial_{yy})\phi = 0. \quad (10)$$

Ignoring this geometrical compatibility constraint and minimizing the free energy directly would lead to the incorrect result that e_1 and e_2 are identically zero, and ϕ (the only field directly coupled to the composition) trivially responds to the local disorder. We can explicitly account for the compatibility constraint by appending it to the free energy (1) via a Lagrange multiplier, $\lambda(\mathbf{x})$. It is then possible to solve for e_1 and e_2 because we have two constraints relating the three strain fields: the compatibility condition (10) and the requirement that the free energy is minimized. Solving for e_1 and e_2 in terms of the order parameter ϕ , we are able to express the free energy in terms of ϕ alone. The contributions

of e_1 and e_2 to the free energy will be accounted for⁴⁶ by terms which have the appearance of a non-local interaction coupling $\phi(\mathbf{x})$ and $\phi(\mathbf{x}')$. Note, by integrating out e_1 and e_2 from the free energy in this way, we are not resorting to an approximation of infinite anisotropy, we are simply analytically solving for the fields e_1 and e_2 in terms of an arbitrary ϕ field.

Proceeding, we find the solutions of the two secondary strain fields e_1 and e_2 which minimize the free energy for a given field ϕ subject to the compatibility constraint. In the standard way, we extremize the free energy with respect to variations in the strain fields, and find Euler-Lagrange “equations of motion” relating the two secondary strain fields to ϕ . Introducing variations δe_1 , δe_2 , and $\delta \lambda$ into (1) yields

$$\begin{aligned} \delta f = & A_1 e_1 \delta e_1 + A_2 e_2 \delta e_2 + \lambda \left\{ \nabla^2 \delta e_1 - \sqrt{8} \partial_{xy} \delta e_2 \right\} \\ & + \delta \lambda \left\{ \nabla^2 e_1 - \sqrt{8} \partial_{xy} e_2 - (\partial_{xx} - \partial_{yy}) \phi \right\} \end{aligned} \quad (11)$$

Doing the requisite integrations by parts, and requiring that δf is zero, we find the following Euler–Lagrange “equations of motion”:

$$e_1 = \frac{-1}{A_1} (\nabla^2 \lambda) \quad (12a)$$

$$e_2 = \frac{\sqrt{8}}{A_2} (\partial_{xy} \lambda) \quad (12b)$$

where λ is given by:

$$-\frac{1}{A_1} (\nabla^2) (\nabla^2 \lambda) - \frac{8}{A_2} (\partial_{xxyy} \lambda) = (\partial_{xx} - \partial_{yy}) \phi \quad (12c)$$

This opaque set of equations becomes quite transparent after reexpressing in \mathbf{k} -space:

$$\tilde{\lambda}(\mathbf{k}) = \frac{(k_x^2 - k_y^2)}{(k_x^2 + k_y^2)^2/A_1 + 8(k_x^2 k_y^2)/A_1} \tilde{\phi}(\mathbf{k}) \quad (13a)$$

$$\tilde{e}_1(\mathbf{k}) = \frac{(k_x^2 + k_y^2)(k_x^2 - k_y^2)/A_1}{(k_x^2 + k_y^2)^2/A_1 + 8(k_x^2 k_y^2)/A_2} \tilde{\phi}(\mathbf{k}) \quad (13b)$$

$$\tilde{e}_2(\mathbf{k}) = \frac{-\sqrt{8}(k_x k_y)(k_x^2 - k_y^2)/A_2}{(k_x^2 + k_y^2)^2/A_1 + 8(k_x^2 k_y^2)/A_2} \tilde{\phi}(\mathbf{k}) \quad (13c)$$

The free energy, which is now a functional of ϕ alone, now may be expressed

$$F = \iint d\mathbf{r} d\mathbf{r}' f_1(\mathbf{r}, \mathbf{r}') \phi(\mathbf{r}) \phi(\mathbf{r}') + \iint d\mathbf{r} d\mathbf{r}' f_2(\mathbf{r}, \mathbf{r}') \phi(\mathbf{r}) \phi(\mathbf{r}') \\ + \int f_{local}(\phi(\mathbf{r})) d\mathbf{r} \quad (14)$$

where f_{local} is the part of the free energy (1) which is explicitly dependent on ϕ alone. The non-local interactions f_1 and f_2 account for the free energy contribution due to the e_1 and e_2 strain fields, respectively. They are given by

$$f_1(\mathbf{r}, \mathbf{r}') \equiv \int \frac{d\mathbf{k}}{a} \frac{A_1}{2} \left[\frac{(k_x^2 + k_y^2)(k_x^2 - k_y^2)/A_1}{8(k_x^2 k_y^2)/A_2 + (k_x^2 + k_y^2)^2/A_1} \right]^2 e^{i\mathbf{k} \cdot (\mathbf{r} - \mathbf{r}')} \quad (15a)$$

and

$$f_2(\mathbf{r}, \mathbf{r}') \equiv \int \frac{d\mathbf{k}}{a} \frac{A_2}{2} \left[\frac{\sqrt{8}(k_x k_y)(k_x^2 - k_y^2)/A_2}{8(k_x^2 k_y^2)/A_2 + (k_x^2 + k_y^2)^2/A_1} \right]^2 e^{i\mathbf{k} \cdot (\mathbf{r} - \mathbf{r}')} \quad (15b)$$

where a is the system area. More transparently, we can write

$$F_1 = \int \frac{d\mathbf{k}}{a} \frac{A_1}{2} \left[\frac{(k_x^2 + k_y^2)(k_x^2 - k_y^2)/A_1}{8(k_x^2 k_y^2)/A_2 + (k_x^2 + k_y^2)^2/A_1} \right]^2 |\phi(\mathbf{k})|^2 \quad (15a)$$

and

$$F_2 = \int \frac{d\mathbf{k}}{a} \frac{A_2}{2} \left[\frac{\sqrt{8}(k_x k_y)(k_x^2 - k_y^2)/A_2}{8(k_x^2 k_y^2)/A_2 + (k_x^2 + k_y^2)^2/A_1} \right]^2 |\phi(\mathbf{k})|^2 \quad (15b)$$

These terms are thus simple harmonic terms, where the bare elastic constants A_1 and A_2 are now \mathbf{k} -dependent. The harmonic term in ϕ is now

$$\int \frac{d\mathbf{k}}{a} \frac{A_\phi(\mathbf{k})}{2} |\phi(\mathbf{k})|^2 \quad (16)$$

with the restoring force $A_\phi(\mathbf{k})$ given by

$$A_\phi(\mathbf{k}) = A_\phi + A_1 Q_1(\mathbf{k})^2 + A_2 Q_2(\mathbf{k})^2 \quad (17)$$

where

$$Q_1(\mathbf{k}) \equiv \frac{(k_x^2 + k_y^2)(k_x^2 - k_y^2)/A_1}{(k_x^2 + k_y^2)^2/A_1 + 8(k_x^2 k_y^2)/A_2} \quad (18a)$$

and

$$Q_2(\mathbf{k}) \equiv \frac{\sqrt{8}(k_x k_y)(k_x^2 - k_y^2)/A_2}{(k_x^2 + k_y^2)^2/A_1 + 8(k_x^2 k_y^2)/A_2}. \quad (18b)$$

The key feature of the harmonic free energy, Eq. (16), is the factor $(k_x^2 - k_y^2)$ buried in Eqs. (18), which leads in a natural way to a tweedy deformation, as follows.

One can immediately see from eq. (13b) and Eq. (13c) that strains e_1 and e_2 will be generated by non-zero $\phi(\mathbf{k})$, *except* for Fourier components for which $k_x^2 - k_y^2 = 0$. Equivalently, one can see from (15a) and (15b) that only Fourier components of $\phi(\mathbf{k})$ with $k_x^2 - k_y^2 = 0$ will incur no free energy cost through the terms f_1 and f_2 , and that their contributions to the harmonic restoring force (17) go to zero. As a result, even for finite elastic anisotropy, non-diagonal Fourier components of ϕ with $k_x^2 - k_y^2 \neq 0$ will be suppressed relative to diagonal components, which will be increasingly prominent for increasing anisotropy. The resulting deformation is a tweedy modulation with long but finite diagonal correlations.

The significance of this nonlocal interaction lies partly in the anisotropy of the interaction, as explained above, but also in the range of the interaction. In Figure 10, we plot the numerically integrated function $(f_1 + f_2)$ along the axial and diagonal directions. The interaction strength along the axial directions is positive, strongly suppressing axial correlations. The interaction along the diagonal direction is negative, enhancing diagonal correlations but only insofar as this interaction survives the $k_x^2 - k_y^2$ suppression. (Note, we plot in Figure 10 the absolute magnitude of the interaction strength along the diagonal direction for better comparison). As one can see from the figure, this long-range interaction dies off like $1/r^2$, and would produce logarithmic divergences in a poorly accommodated two dimensional system. The inevitable result is the development of extended, coordinated lattice modulations which take advantage of the compositional disorder (or any other driving

force which couples to the martensitic strain) without generating unnecessary strains: i.e. tweed.

Alternative Couplings

In the preceeding section, we have reexpressed the simple physics embodied in continuum elasticity in a manner which emphasizes the long-range, collective nature of the lattice's response to a perturbing force. In particular, this approach helps to clarify why a tweedy modulation is the natural response of a system in which a disorder field is coupled to the strain. We will here briefly consider possible couplings between the disorder field and the strain, and argue that the coupling incorporated into the present model, i.e. the term $\eta\phi^2$ is most effective at generating tweed and most appropriately describes the experimental observations.

We have noted that the simplest coupling between the martensitic strain ϕ and the composition η is $\eta\phi^2$, prompting its inclusion in our Landau free energy via the term $A_\eta \delta\eta \phi^2$. While it is true that this is the simplest coupling between a scalar field and the order parameter ϕ , our decision to consider a *scalar* field coupled directly to the ϕ component of the strain field requires justification, since non-scalar disorder fields and the other strain components can not in principle be neglected out of hand.

First, we've chosen to couple to ϕ directly for the same reason that we've taken it as our order parameter and included its anharmonic terms: ϕ is the predominant strain measured in the tweed deformation and it is the strain responsible for the martensitic transformation. As such, it is larger in magnitude than the other strain components and will be most susceptible to interacting with a driving force, whether due to intrinsic disorder or some extrinsic field such as an externally applied stress.

Second, we've chosen a scalar disorder field simply because tweed is so impressively widespread a phenomena, and we desire to study the simplest, most universal disorder.

Indeed, there are important materials with unit cell configurations that allow for some disorder field more complicated than simply scalar: the obvious example is oxygen concentration in YBCO. However, we find it provocative that tweed appears in materials with even simple lattices such as FCC or BCC. Here, disorder takes the form of random placement of atoms, with each site being symmetrically equivalent with every other. In this case, disorder is necessarily simply a scalar field for which the broken symmetry of the martensitic strain precludes a linear coupling. Even in the case of nickel-rich $\text{Ni}_x\text{Al}_{1-x}$, which has an ordered β -CsCl structure, the compositional disorder can be described by a scalar field corresponding to the positions of the excess nickel atoms, which are accommodated by random substitution onto the aluminum sublattice⁴⁷.

Third, we know that composition couples not only to the martensitic transformation strain, but to the martensitic transformation *temperature*. Compositional inhomogeneities will result in a spatially varying transformation temperature, and in a ϕ^6 Landau free energy this is reflected in spatial variations in the coefficient of ϕ^2 .

Fourth, the experimental observation of hysteresis immediately allows us to conclude that a simple linear response mechanism cannot be the general origin of tweed. Hysteresis is seen⁸ to occur upon cycling of temperature: upon heating, the tweed pattern persists up to a temperature which is higher than that at which it initially appeared upon cooling. This hysteresis implies that the tweed is something more complex than simply linear response of the lattice to some static defect or impurity. In linear response, the lattice displacements are calculated as a single-valued function of the perturbing force, and the tweed would therefore form and fade without history dependence. The temperature dependence of the tweed pattern would arise from the (single-valued) temperature dependence of the elastic constants, and it is difficult to conceive of a possible source of hysteresis in this mechanism.

Having given the above justification for the $\eta\phi^2$ coupling which we have investigated in detail, we would like to go on to consider other possible couplings.

Coupling to Order Parameter Linearly: The system in which tweed has received the greatest amount of attention in the last several years is the high temperature superconductors. In the YBCO type materials, there are twice as many oxygen sites in the Cu-O planes as oxygen atoms, and the tetragonal to orthorhombic martensitic transition occurs as the randomly distributed oxygen atoms break the twofold symmetry between sites and preferentially align along one axis. This alignment results in an increased lattice constant in one direction relative to the other, and a net rectangular deformation in the Cu-O plane. In this case, if the oxygen distribution is taken as the disorder field, disorder clearly couples directly to ϕ , and the corresponding term in a Landau free energy describing this system would appear as a term linear in disorder and strain, $\eta\phi$. Even though the coupling is linear, it is conceivable that hysteresis may arise from the complicated dynamics of the diffusing oxygen.

This model has been extensively studied. Semenovskaya *et al.*^{18,48} and Parlinski *et al.*¹⁹ have each considered a model for YBCO in which diffusing oxygen atoms arrange into martensitic microdomains, and the coupling between oxygen position and elastic strain leads directly to an unquestionably tweedy lattice deformation. Morphologically, the tweed structures found in these studies is essentially identical to that presented in this paper; not only is the qualitative appearance identical, but quantitatively the correlation lengths are comparable as well. However, there is a fundamental difference in the *physical nature* of the tweed structures. In their investigations, the tweed is not an equilibrium phase, but rather a non-equilibrium or metastable configuration. Semenovskaya *et al.*¹⁸ observe tweed as an intermediate structure as the oxygen distribution gradually evolves through an ordering process, passing through a transient stage (or getting stuck in a metastable well) consisting of highly anisotropic microdomains before ultimately reaching the equilibrium twinned martensitic configuration. In addition to this transient tweed, Parlinski *et al.* also find “embryonic” tweed resulting from thermal fluctuations *above* the transition temperature,

which they treat analytically as critical fluctuations in a second order transition. These studies have produced a dynamic or metastable tweed in contrast to the static equilibrium tweed phase which our model seeks to explain. Yet, despite the compelling analogy, it is not quite accurate to infer they have produced the liquid out of which our glass forms!

The nature of the disorder in their nonequilibrium tweed is fundamentally different from the nature of the disorder in our equilibrium tweed. The distribution of oxygen atoms constitutes their disorder: randomly scattered or clustered into microdomains or ordered into martensitic variants, the oxygen atoms couple to the strain and give rise to some lattice deformation. Yet, since the oxygen atoms diffuse in response to external parameters, *oxygen is not a source of quenched-in disorder*. The oxygen is effectively an additional degree of freedom which the system integrates out as it searches for a stable equilibrium. In this light, it is clear why there is no stable, static, equilibrium tweed phase to be found in these models. In contrast, the model presented in this paper relies on the presence of intrinsic quenched-in disorder, in the form of static compositional inhomogeneities, in order to stabilize the tweed phase.

Why then, is static tweed seen in YBCO at all? Significantly, it is when YBCO is doped with an impurity that static tweed appears. After substituting copper with as little as 1.5% of a transition metal element (such as Fe, Co, Al, or Ga), TEM observations of tweed are made¹³. These impurity atoms are frozen in at temperatures well above the tweed regime¹³, typically at $> 700K$, and therefore the impurity disorder is truly quenched-in. Studies by Jiang *et al.*⁴⁹ and Krekels *et al.*⁵⁰ have demonstrated static microdomain formation due to quenched-in impurity atoms. In these studies, the oxygen–copper and oxygen–impurity interactions are such that the impurity atoms, which prefer nearest-neighbor oxygen occupancy, confound the oxygen chain alignment preferred by the surrounding matrix of copper atoms⁵¹. It is through the compromise arrangement of the oxygen atoms that the static impurity disorder is communicated to the elastic

deformation. Recent simulation studies by Semenovskaya *et al.*⁴⁸ have included quenched-in impurities as well as the long-range strain interactions, and have indeed generated a static, apparently stable, tweed phase. Ultimately, in such a model, the impurity atoms act as sites favoring the square phase amid copper sites favoring the rectangular phase. The compositional variation therefore selects a phase (square or rectangular) but it does not select a particular martensitic variant: the symmetry of a copper site within the unit cell prevents it from coupling linearly to the rectangular strain. It is just this physical situation which is represented in our general model by a quadratic coupling between compositional disorder η and rectangular strain ϕ . The present study, which seeks to clarify the general principle involved in equilibrium tweed, and the studies cited above, which seek to elaborate in valuable detail the specific mechanism at work in the case of YBCO, therefore complement each other very well.

Coupling to Gradients of Disorder: Although the disorder on an atomic scale can be described by a scalar field, it is possible for the random compositional variations to conspire to produce clusters of more complex symmetry, which may then collectively couple to the order parameter. For example, as Robertson and Wayman⁶ have argued with respect to NiAl, random clusters of nickel atoms have a high probability of having tetragonal symmetry, and therefore coupling to the martensitic strain. In the language of the Landau–Ginzburg formalism, this corresponds to a coupling between higher order gradients of the disorder field and the order parameter.

In two dimensions, the term $\phi(\partial_x^2 - \partial_y^2)\eta$ is a symmetry-allowed coupling between η and ϕ which is *a priori* no less important than the quadratic coupling we have used. Since this term is only linear in ϕ , it could well be comparable in magnitude to the quadratic coupling, despite the second derivative, and be just as effective in generating some lattice deformation. The relevant question, however, is: what is the capacity of such a term to generate *tweed*. This is most easily answered by reexpressing the term in k-space:

$\tilde{\phi}(\mathbf{k})(k_x^2 - k_y^2)\tilde{\eta}(\mathbf{k})$. Recall that tweed is correlated along diagonal directions, and therefore is composed of fourier components for which $k_x^2 - k_y^2 \rightarrow 0$. Therefore, although $(\partial_x^2 - \partial_y^2)\eta$ couples to the order parameter, it does not do so in a manner which allows it to generate tweed. (In three dimensions, a slightly more involved calculation²⁹ leads to the same result.)

Coupling to Bulk Dilation: Perhaps the most commonly considered deformation due to compositional disorder is that which arises from atomic size mismatch in alloys. This mechanism is represented by the coupling ηe_1 between composition and bulk dilation, and although it does not directly couple η and ϕ , we have repeatedly emphasized that the strain fields are not independent and are intrinsically coupled by the compatibility conditions.

In the previous section, we were able to translate the bulk dilation and diagonal strain contributions to the free energy into non-local interactions in ϕ , by integrating those secondary strains out of the free energy, subject to the compatibility constraint. We can carry out the analogous analysis for a term $D\eta e_1$, as follows:

The variation in the free energy caused by variations δe_1 , δe_2 , and $\delta \lambda$ is

$$\begin{aligned} \delta f = & (A_1 e_1 + D\eta)\delta e_1 + A_2 e_2 \delta e_2 + \lambda \left\{ \nabla^2 \delta e_1 - \sqrt{8} \partial_{xy} \delta e_2 \right\} \\ & + \delta \lambda \left\{ \nabla^2 e_1 - \sqrt{8} \partial_{xy} e_2 - (\partial_{xx} - \partial_{yy}) \phi \right\} \end{aligned} \quad (19)$$

and the corresponding expressions for e_1 , e_2 , and λ are

$$e_1 = \frac{-1}{A_1}(\nabla^2 \lambda - D\eta) \quad (20a)$$

$$e_2 = \frac{\sqrt{8}}{A_2}(\partial_{xy} \lambda) \quad (20b)$$

$$-\frac{1}{A_1}(\nabla^2)(\nabla^2 \lambda + D\eta) - \frac{8}{A_2}(\partial_{xxyy} \lambda) = (\partial_{xx} - \partial_{yy})\phi. \quad (20c)$$

In k-space this gives us

$$\tilde{\lambda}(\mathbf{k}) = \frac{(k_x^2 - k_y^2)\tilde{\phi}(\mathbf{k}) + (k_x^2 + k_y^2)D\tilde{\eta}(\mathbf{k})/A_1}{(k_x^2 + k_y^2)^2/A_1 + 8(k_x^2 k_y^2)/A_1} \quad (21a)$$

$$\tilde{e}_1(\mathbf{k}) = \frac{(k_x^2 + k_y^2)(k_x^2 - k_y^2)\tilde{\phi}(\mathbf{k})/A_1 - (k_x^2 k_y^2)D\tilde{\eta}(\mathbf{k})/A_1 A_2}{(k_x^2 + k_y^2)^2/A_1 + 8(k_x^2 k_y^2)/A_2} \quad (21b)$$

$$\tilde{e}_2(\mathbf{k}) = \frac{-\sqrt{8}(k_x k_y)(k_x^2 - k_y^2)\tilde{\phi}(\mathbf{k})/A_2 - (k_x k_y)(k_x^2 + k_y^2)D\tilde{\eta}(\mathbf{k})/A_1 A_2}{(k_x^2 + k_y^2)^2/A_1 + 8(k_x^2 k_y^2)/A_2} \quad (21c)$$

Again, the free energy can now be written in terms of ϕ alone. The contributions due to $A_1 e_1^2$ and $A_2 e_1^2$ are identical to those found in the previous section, as they must be, with the terms proportionate to $\tilde{\eta}$ cancelling. The contribution from the disorder term, $D\eta e_1$ is now a non-local interaction between disorder and ϕ (where the term quadratic in disorder can be dropped by redefining the zero of the energy):

$$F_\eta = \iint d\mathbf{r} d\mathbf{r}' f_\eta(\mathbf{r}, \mathbf{r}') \phi(\mathbf{r})\eta(\mathbf{r}') \quad (22)$$

where

$$f_\eta = \int \frac{d\mathbf{k}}{a} \frac{D}{A_1} \frac{(k_x^2 + k_y^2)(k_x^2 - k_y^2)}{(k_x^2 + k_y^2)^2/A_1 + 8(k_x^2 k_y^2)/A_2} e^{i\mathbf{k} \cdot (\mathbf{r} - \mathbf{r}')} \quad (23)$$

More transparently, we can write

$$F_\eta = \int \frac{d\mathbf{k}}{a} \frac{D}{A_1} \frac{(k_x^2 + k_y^2)(k_x^2 - k_y^2)}{(k_x^2 + k_y^2)^2/A_1 + 8(k_x^2 k_y^2)/A_2} \tilde{\phi}(\mathbf{k}) \tilde{\eta}(-\mathbf{k}). \quad (24)$$

In the previous section we casually argued that a term like this one will be ineffective in generating a tweedy deformation because it vanishes precisely for those Fourier modes ($k_x \simeq \pm k_y$) which correspond to tweed. A more careful analysis would account for the fact that the restoring force $A_\phi(\mathbf{k})$ is \mathbf{k} -dependent, and diminishes as $k_x \pm k_y \rightarrow 0$, *enhancing* the effectiveness of this driving force. The term in the last section turns out to indeed be harmless, but here we give a more complete analysis. Within linear elasticity, it is possible to solve explicitly for the deformation resulting from Eq. (24).

We are considering the harmonic free energy

$$F = \int \frac{d\mathbf{k}}{a} \frac{A_\phi(\mathbf{k})}{2} |\phi(\mathbf{k})|^2 + D Q_1(\mathbf{k}) \tilde{\phi}(\mathbf{k}) \tilde{\eta}(-\mathbf{k}) \quad (25)$$

where $A_\phi(\mathbf{k})$ and $Q_1(\mathbf{k})$ defined in Eqs. (17) and (18a) respectively. This is minimized when

$$\tilde{\phi}(\mathbf{k}) = \frac{-D Q_1(\mathbf{k}) \tilde{\eta}(-\mathbf{k})}{A_\phi(\mathbf{k})}. \quad (26)$$

The most revealing measure of this simple result is the corresponding diffraction pattern for a white disorder distribution $\eta(\mathbf{k}) = \eta$, which we calculate using

$$\begin{pmatrix} \tilde{\phi}(\mathbf{k}) \\ \sqrt{2} \tilde{e}_2(\mathbf{k}) \end{pmatrix} = \frac{1}{\sqrt{2}} \begin{pmatrix} k_x & -k_y \\ k_y & k_x \end{pmatrix} \begin{pmatrix} U_x(\mathbf{k}) \\ U_y(\mathbf{k}) \end{pmatrix} \quad (27b)$$

and

$$\tilde{e}_2(\mathbf{k}) = -Q_2(\mathbf{k}) \tilde{\phi}(\mathbf{k}) - \frac{D\eta}{A_1} Q_3(\mathbf{k}) \quad (28)$$

where

$$Q_3(\mathbf{k}) = \frac{(k_x k_y)(k_x^2 + k_y^2)/A_2}{(k_x^2 + k_y^2)^2/A_1 + 8(k_x^2 k_y^2)/A_2}. \quad (29)$$

We can invert Eqs. (27) and use Eqs. (26) and (28) to find

$$\begin{pmatrix} U_x(\mathbf{k}) \\ U_y(\mathbf{k}) \end{pmatrix} = \frac{\sqrt{2}}{k^2} \begin{pmatrix} k_x & k_y \\ -k_y & k_x \end{pmatrix} \begin{pmatrix} \frac{-D\eta Q_1(\mathbf{k})}{A_\phi(\mathbf{k})} \\ \sqrt{2} \left\{ \frac{D\eta Q_1(\mathbf{k}) Q_2(\mathbf{k})}{A_\phi(\mathbf{k})} - \frac{D\eta}{A_1} Q_3(\mathbf{k}) \right\} \end{pmatrix} \quad (30)$$

The scattering contours in figure 11 were calculated from the solution (30) to the linear problem. For finite anisotropy, the diffuse scattering deviates substantially from that expected from tweed, showing that a substantial amount of non-tweedy deformation is occurring in the lattice.

This is in agreement with the much earlier analysis of Cochran and Kartha⁵² who show that the long-range strain field associated with random variation in bulk dilation will lead to diffuse scattering with a strong radial component at $\langle 0h \rangle$ Bragg peaks. This is qualitatively distinct from the diagonal diffuse streaking seen in tweed. As the anisotropy increases however, the diffuse scattering lobes converge toward the diagonal directions, and grow increasingly similar to the diagonal streaks associated with tweed.

This suggests that within linear elasticity a coupling ηe_1 between disorder and bulk dilation is ineffective at generating tweed for most realistic materials parameters. As a more fair test of this coupling, we must also determine whether tweed might still appear in the full non-linear model that includes terms anharmonic in the ϕ strain. Of course, an analytical solution is now unfortunately inaccessible, but introducing the coupling to bulk dilation into our numerical simulation with finite anisotropy, we've determined that this coupling does not result in a identifiably tweedy modulation. The configuration in Figure 12 was obtained by eliminating the coupling $\eta\phi^2$ and replacing it with a coupling ηe_1 of the same strength. The lattice is noticeably deformed, yet the modulations clearly do not constitute tweed.

Conclusion

We have reported the results of a simulation of the pretransitional behavior of a two dimensional martensitic model material. Unlike the historically traditional procedure of seeking and studying in local detail the coupling of special localized defects to first order transitions, we show that intrinsic statistical variation of composition suffices to generate tweed patterns, as well as to provide an understanding of how a tweed region can exist in a transitional regime over an extended temperature range above the nominal bulk transformation temperature. Most importantly, the model described here has uncovered a tweed that is far more complex than a mere lattice response to local defects. Long-range, cooperative, non-linear processes give rise to tweed which is, in the infinite anisotropy limit, a distinct stable thermodynamic phase between the austenite and martensite phases, and which is moreover a glass phase that exhibits properties distinct from the phases it separates: slow relaxation, a diverging non-linear susceptibility, glassy dynamics. In actual materials which do not have infinite anisotropy, the phase transitions bounding the glassy phase will be rounded, but many real-world materials are indeed anisotropic enough that the tweed regime is likely to still exhibit experimentally observable glassy behavior.

From the modeling point of view we have once again demonstrated the utility of non-linear, nonlocal free energy functions, now extended to non-uniform, disordered systems, for representing the mesoscale phenomenology of patterns in lattice distortive phase transitions. This formalism makes contact with a wide class of other displacive transitions in metals, non-metals and ceramics, e.g. ferroelectricity, ferroelasticity, perhaps even biomolecular conformation changes³¹. It has been our aim in this paper to outline the method in sufficient detail that it can now be applied to various materials, at least semi-quantitatively.

A logical continuation of the present research would, of course, extend this model and simulation to three dimensions. Like many attempts to address pretransitional mesoscale modulations, this approach casually seeks to investigate a three dimensional phenomena with a two dimensional model, and various problems arise with this uncontrolled approximation. A two dimensional system will certainly be more unstable toward a lattice distortion such as tweed than a real three dimensional material. (Indeed, in two dimensions there is generally *no* stable finite temperature crystalline phase.) Also, in attempting to describe a three dimensional material with a two dimensional model, one must use materials parameters from the real material, and hope that the model will yield similar behavior, but it is possible that qualitatively different physics may be important in the real 3D sample. For example, in modeling planar compounds such as the high T_c materials, such a two dimensional approach still incorporates the appropriate physical symmetries. On the other hand, cubic materials have additional compatibility conditions and the limit of infinite elastic anisotropy yields a six component Potts-like model rather than an Ising model²⁹. We have yet to investigate how this may cause tweed in cubic materials to differ from tweed in tetragonal materials.

An additional issue deserving further research is the softening behavior in the pretransitional tweed regime. We have long suspected that the pretransitional “anomalies” in

elastic constant behavior are inextricably connected to the presence of tweed type modulations. Whereas conventional wisdom holds that elastic softening leads to pretransitional modulations (and ultimately to the martensitic transformation), we believe that the softening can in turn be *enhanced* by the pretransitional modulation. A bulk elastic constant, measured over an entire macroscopic specimen, will necessarily reflect not simply the harmonic response arising from the bare interatomic potentials, but also the mesoscopic lattice response to the applied driving force. When stressed, a modulation such as tweed will certainly respond elastically, but it will also flip domains, depin boundaries, rearrange clusters etc. We believe that it is precisely such nonlinear processes which account for much of the behavior underlying the pretransitional anomalies in elastic softening, internal friction, and acoustic attenuation. We’ve undertaken to investigate these effects in our model by studying the response of a simulated patch of tweed to an externally applied strain. Allowing these relaxational processes, we measure elastic constants which are substantially softer than the “bare” elastic constants otherwise found. Furthermore, we observe the dissipative and hysteretic effects which underlie the experimental ultrasonic attenuation and internal friction measurements²⁹.

Many of the ideas which have been incorporated into this model have also been of central importance in earlier work by a number of other investigators. Ericksen³² and Jacobs²¹ have considered the limit of infinite anisotropy and shown the general form for allowed solutions. Semenovskaya *et al.* and Parlinski *et al.* have noted the vital importance of the long-range nature of strain fields in a lattice modulation such as transient¹⁸ and dynamical¹⁹ tweed. Jiang *et al.*¹⁴, Krekels *et al.*⁵⁰ and Becquart *et al.*⁴ have recognized the importance of compositional randomness (i.e. random placement of alloy components or dopants) in determining the tweed structure. We have assembled these various ingredients into a strikingly simple and powerfully general model which provides compelling answers to two questions which have been troubling investigators of pretransitional phenomena in

martensitic materials for many years: What is tweed? Why does it occur? Moreover, the answers given here have established an unexpected connection between tweed and spin glasses, suggesting a new line of experimental investigation into tweed. The signature of glassiness may be observable in tweed through measurements of nonlinear elastic constants at the onset of tweed, measurements of frequency dependent relaxation phenomena using ultrasonic attenuation, or investigations of “remanent strain” through hysteresis measurements, for example. In establishing this connection between tweed and glasses, it is hoped that the tools being developed within the field of disordered systems in condensed matter theory may be brought to bear on the problem of pretransitional phenomena in martensitic systems.

We would like to thank Lee Tanner for helpful and enjoyable discussions, and for providing the TEM image used in Figure 1. We also thank Teresa Castán, who was a very welcome collaborator in the spin glass aspects of this research. We acknowledge the support of DoE Grant #DE-FG02-88-ER45364. SK also acknowledges support from the Department of Education and from the Sloan Foundation, Grant #93-6-6.

REFERENCES

1. Figure 1 appears courtesy of Lee Tanner.
2. S. Kartha, T. Castan, J. A. Krumhansl, and J. P. Sethna, *Phys. Rev. Let.*, **67**, (1991), 3630. J. P. Sethna, S. Kartha, T. Castán, and J. A. Krumhansl, *Physica Scripta*, **T42**, (1992), 214.
3. A. Heiming, W. Petry, J. Trampenau, M. Alba, C. Herzig, H. R. Schober, G. Vogl, *Phys. Rev. B*, **43**, (1991) 10948. See also parts I and II of this series, *Phys. Rev. B*,

- 43**, (1991) 10933 and 10963.
4. C. S. Becquart, P. C. Clapp, and J. A. Rifkin, *Phys. Rev. B*, **48**, (1993), 7.
 5. L. E. Tanner, M. Wuttig, *Mat. Sci. and Eng.*, **A127**, (1990) 137.
 6. I. M. Robertson and C. M. Wayman, *Phil. Mag. A*, **48**, (1983) 421, 443, 629. D. Schryvers and L. E. Tanner, *Ultramicroscopy*, **37**, (1990) 241). L. E. Tanner, D. Schryvers and S. M. Shapiro, *Mater. Sci. Eng. A*, (1990) 205.
 7. S. Muto, S. Takeda, R. Oshima, and F. Fujita, *J. Phys: Cond. Mat.*, **1**, (1989) 9971. S. Muto, S. Takeda and R. Oshima, *Jap. J. Appl. Phys.*, **29**, (1990), 2066.
 8. R. Oshima, M. Sugiyama, and F. E. Fujita, *Met. Trans. A*, **19**, (1988) 803.
 9. S. Muto, R. Oshima, and F. Fujita, *Acta Metall. Mater.*, **4**, (1990), 685.
 10. K. Yosuda and Y. Kanawa, *Trans. Jap. Inst. Metals*, **18**, (1972) 46.
 11. T. Onozuko, N. Ohnishi and M. Hirabayahsi, *Metall. Trans. A+*, **19**, (1988) 797.
 12. W. W. Schmahl, A. Putnis, E. Salje, P. Freeman, A. Graeme-Barber, R. Jones, K. K. Singer, J. Blunt, P. P. Edwards, J. Loram, and K. Mirza, *Phil. Mag. Let.*, **60**, (1989) 241. T. Krekels, G. van Tendeloo, D. Broddin, S. Amelinckx, L. Tanner, M. Mehbod, E. Vanlathem, and R. Deltour, *Physica C*, **173**, (1991) 361;
 13. Y. Zhu, M. Suenaga, and J. Tafto, *Phil. Mag. Let.*, **64**, (1991), 29. Y. Zhu, M. Suenaga, and A. R. Moodenbaugh, *Phil. Mag. Let.*, **62**, (1990), 51. Y. Xu, M. Suenaga, J. Tafto, R. L. Sabatini, and A. R. Moodenbaugh, *Phys. Rev. B*, **39**, (1989), 6667.
 14. X. Jiang, P. Wochner, S. C. Moss, and P. Zschack, *Phys. Rev. Let.*, **67**, 2167, (1991). *Proceedings of International Conference on Martensitic Transformations*, Monterey, CA. 20-24 July, 1992.

15. A. H. Heuer, R. Chaim, and V. Lanteri, *Adv. in Ceramics*, **24**, (1988) 3; A. H. Heuer and M. Rhüle, *Acta Met.*, **12**, (1985) 2101.
16. L. Tanner, *Phil. Mag.*, **14**, (1966), 111.
17. G. R. Speich and K. A. Taylor, in *Martensite*, eds. G. B. Olson and W. S. Owen, (ASM International, 1992), 243.
18. S. Semenovskaya and A. G. Khachaturyan, *Phys. Rev. Let.*, **67**, (1991), 2223. L.-Q. Chen, Y. Wang, and A. G. Khachaturyan, *Phil. Mag. Let.*, **65**, (1992), 15. S. Semenovskaya, and A. G. Khachaturyan, *Physica D*, **66**, (1993), 205.
19. K. Parlinski, E. K. H. Salje, and V. Heine, *Acta Metall. Mater.*, **41**, (1993), 839. K. Parlinski, V. Heine, and E. K. H. Salje, *J. Phys.: Condens. Matter*, **5**, (1993), 497. E. Salje and K. Parlinski, *Supercond. Sci. Technol.*, **4**, (1991), 93. A. M. Bratkovsky, S. C. Marais, V. Heine, and E. K. H. Salje, *J. Phys.: Condens. Matter*, **6**, (1994), 3679.
20. F. Falk, *Z. Phys. B - Condensed Matter*, **51**, (1983), 177.
21. A. E. Jacobs, *Phys. Rev. B*, **31**, (1985), 5984.
22. The analogous mechanism in the case of the random field Ising model has been investigated by Y. Imry and M. Wortis, *Phys. Rev. B*, **19**, (1979), 3580.
23. This model is appropriate to so-called “proper” ferroelastics, in contrast to improper ferroelastics where some “shuffle” or optical mode distortion drives the transition⁵⁵.
24. L.D.Landau and D.M.Lifshitz, *Statistical Physics*, (Pergamon, Oxford, 1968), 2nd ed.
25. It is important to note that this softening is not a complete softening to zero frequency. The sixth order expression for the energy of the ϕ strain gives a triple well

potential where the wells at $\phi = \pm\phi_M$ become the thermodynamically stable phase when the quadratic coefficient is *still positive*, i.e. this is a first-order transformation and occurs with only a partial softening of A_ϕ ^{54,30}. Indeed some ferroelastic transitions are true soft mode transitions, but then these are truly second order and the attendant critical fluctuations will naturally give rise to some dynamical pretransitional effects.

26. A positive strain gradient coefficient will contribute upward curvature to the dispersion of the related phonon branch^{55,29} (in this case the TA₁ branch). Measuring the curvature in experimental data⁵³ (and accounting for the negative curvature of arising simply from lattice discreteness) yields the strain gradient coefficient we need.
27. Notice that the horizontal axis is not simply the average composition, as is usually the case for binary alloy phase diagrams. Over the range of interest, composition has a simple relationship to transformation temperature, and so no additional information would be revealed. The strength of the coupling reveals more information, and is a more appropriate comparison to previous analytical work, as will be discussed below.
28. The twins form for precisely the same reason that domains form in ferromagnets: elastic strain energy (magnetic field energy) is minimized by setting up alternating martensitic variants (magnetic domains) which partially cancel each other's long-range strain field (magnetic field).
29. S. Kartha, Ph.D. Thesis, Cornell University, 1994, unpublished.
30. J. A. Krumhansl and R. J. Gooding, *Phys. Rev. B*, **39**, (1989), 3047.
31. A. D. Bruce and R. A. Cowley, *Structural Phase Transitions*, (Taylor and Francis, London: 1981).
32. Discussed by J. L. Ericksen, *Int'l J. of Solids and Structures*, **22**, (1986), 951.

33. P. F. Gobin, and G. Guenin, in Solid State Phase Transformations in Metals and Alloys, proceedings of Ecole d'été d'Aussois, Sept. 3-15, 1978, (Les Éditions de Physiques, Orsay, France)
34. This is related to the Edwards-Anderson order parameter in spin glass literature; see, for example, K. Binder and A. P. Young, *Rev. of Mod. Phys.*, **58**, (1986) 801.
35. M. Mezard, G. Parisi, and M. A. Virasoro, *Spin Glass Theory and Beyond*, (World Scientific, Singapore: 1987).
36. The fact that our low temperature correlation data can be fit to a power law does not contradict this assertion, because careful spin glass simulations by Ogielski have also observed apparent power law correlations. (See *Phys. Rev. B*, **32**, (1985), 7384.) The mean-field theoretical prediction is that correlations will have a piece which falls off as $t^{-\nu}$ and a static piece which remains at infinite times. (See H. Sompolinsky and A. Zippelius, *Phys. Rev. B*, **25**, (1982), 6860.)
37. M. Wuttig, *Met. Trans. A*, **19**, (1988) 185.
38. The top set of results in this figure uses the same data which gave long time correlations in Figure 4.
39. J. Van Tendeloo, J. Van Landuyt, and S. Amelinckx in *Competing Interactions and Microstructures: Statics and Dynamics*, ed. by LeSar, R., A. Bishop, and R. Heffner (Springer-Verlag, Berlin: 1988)
40. L.E. Tanner, S. M. Shapiro, D. Shryvers, and Y. Noda, *Mat. Res. Soc. Symp. Proc.*, **246**, (1992), 265.
41. This partially static tweed had a ϕ correlation of $\xi(t = 5000MCS) = .08$.
42. C. Zener, *Phys. Rev.*, **71** (1947) 846.

43. M. A. Krivoglaz, *Theory of X-Ray and Thermal Neutron Scattering by Real Crystals*, (Plenum, New York, 1969).
44. I.S.Sokolnokoff, *Mathematical Theory of Elasticity*, McGraw–Hill, New York (1946).
45. M.Baus and R.Lovett, *Phys. Rev. B*, **65**, (1990), 1781.
46. The computer simulation uses the displacement fields as the degrees of freedom, so this geometric compatibility is automatically guaranteed; it is taken into account implicitly because the simulation algorithm considers distortions of a defect-free lattice.
47. A. Bradley and A. Taylor, *Proc. R. Soc. A.*, **159**, (1937), 56.
48. S. Semenovskaya, and A. G. Khachaturyan, *Phys. Rev. B*, **47**, (1993), 12182.
49. X. Jiang, P. Wochner, S. C. Moss, and P. Zschak, preprint. To appear in *Proceedings of ICOMAT-92*, (Monterey, California, July 20-24, 1992).
50. T. Krekels, G. van Tendeloo, D. Broddin, S. Amelinckx, L. Tanner, M. Mehbod, E. Vanlathem, and R. Deltour, *Physica C*, **173**, (1991), 361.
51. D. De Fontaine, L. T. Wille, and S. C. Moss, *Phys. Rev. B*, **36**, (1987), 5709.
52. W. Cochran and G. Kartha, *Acta Crystallogr.*, **9**, (1956), 259, 941, 944.
53. M. Sato, B. H. Grier, S. M. Shapiro, and H. Miyajima, *J. Phys: Met. Phys.*, **12**, (1982), 2117-2129.
54. G. R. Barsch and J. A. Krumhansl, in *Martensite*, eds. G. B. Olson and W. S. Owen, (ASM International, 1992), 126.
55. G. R. Barsch and J. A. Krumhansl, *Met. Trans. A*, **19A**, (1988), 761.

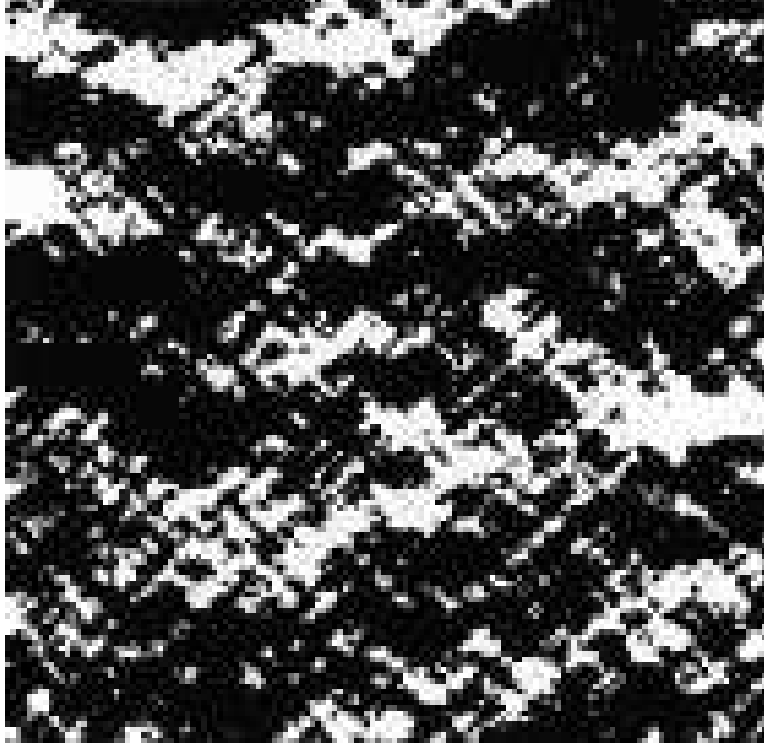


Figure 1. **Tweed:** is shown here as experimentally observed in transmission electron microscopy of NiAl. It is identified by its diagonal striations, which reflect some pseudo-periodic lattice deformation with correlations on the scale of some tens of atomic spacings. This pattern is consistent with simulation results below.

Figure 2(a). **Simulation Results:** These configurations are generated by a Monte Carlo computer simulation based on the continuum elasticity model of a system undergoing a square \rightarrow rectangular martensitic transformation, where the transformation strain has been coupled to a disordered composition field. The shading reflects the strain order parameter $\phi(\mathbf{x})$, varying from dark to light as the strain goes from the horizontally stretched rectangular martensite variant, to undeformed square phase, to the vertically stretched variant. (a) The undeformed austenite phase. (b) Mottled texture. (c) Fine tweed. (d) Coarse tweed. (e) Twinned martensite.

Figure 2(b,c). **Simulation Results.**

Figure 2(d,e). **Simulation Results.**

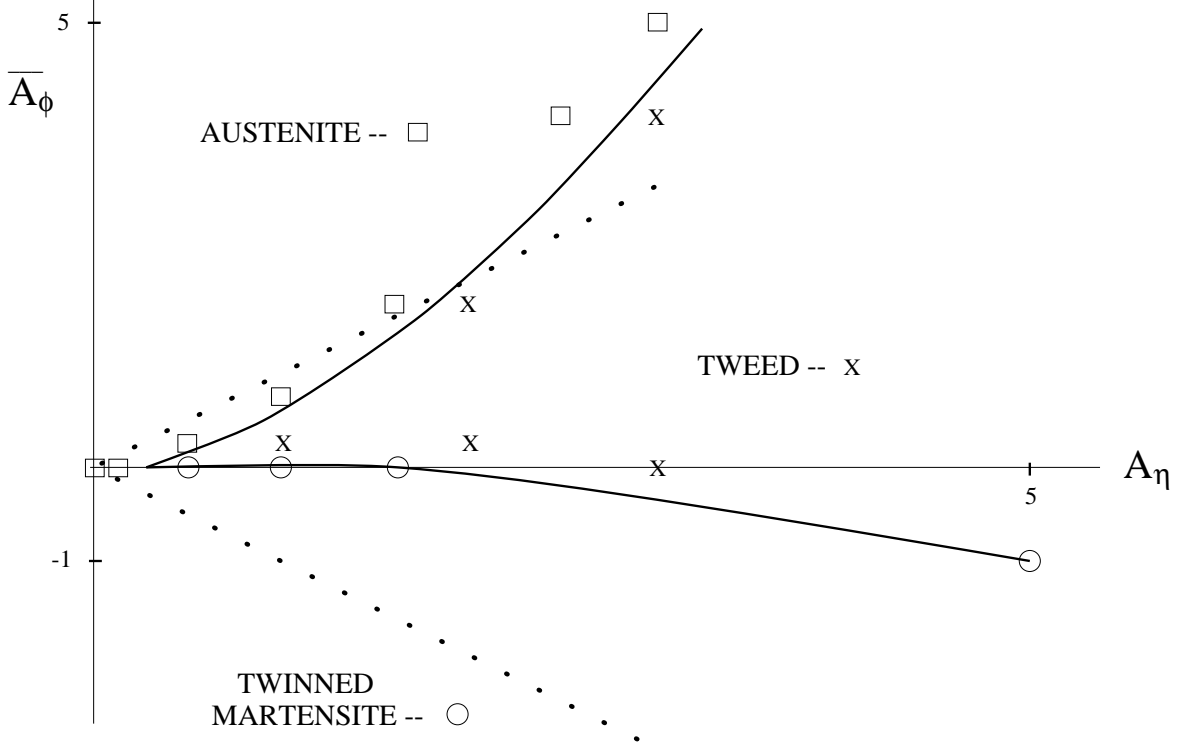


Figure 3. **Phase Diagram** for this model is plotted against parameters \bar{A}_ϕ and A_η (given in units of 10^{10} N/m²). The symbols \square , X, and \circ mark some points in parameter space where the numerically determined groundstate configuration is austenite, tweed, or martensite, respectively. The solid lines are drawn to separate the resulting three regimes: 1) The AUSTENITE phase is the relatively undeformed lattice. 2) The TWEED structure develops as a response to the compositional disorder. The degree of deformation depends on the degree of softening and the strength of the coupling to the disorder field. 3) The TWINNED MARTENSITE is the conventional low temperature phase. The dotted lines correspond to the phase boundaries in the infinite anisotropy approximation, in which the martensitic tweed problem is mapped to a spin glass².

Time Correlations

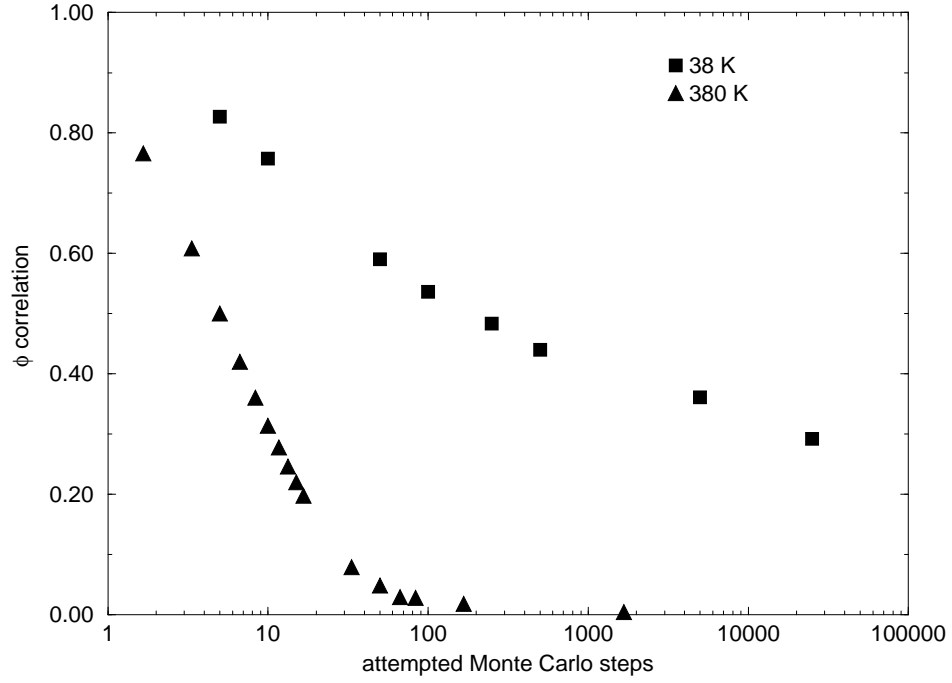


Figure 4. **Time Correlations:** Correlations in the ϕ martensitic distortion as a function of time, (where time is measured in attempted Monte Carlo steps). The physical temperature for each curve is converted from the corresponding Monte Carlo temperature. The upper curve reveals persistent correlations, suggestive of sluggish, glassy dynamics.

Figure 5. **Diffuse Streaking:** around three bragg points is shown. (a) Experimental x-ray scattering data¹⁴ for $\text{YBa}_2\text{Cu}(\text{Al})_3\text{O}_{7-\delta}$ around the indicated Bragg peaks. (b) Corresponding diffraction data extracted from the computer simulation of tweed (using FePd parameters) faithfully reproduce important features of the experimental data, i.e. the diffuse streaking is highly anisotropic, most pronounced in the $\langle 11 \rangle$ directions, and asymmetrically depends on the Bragg peak index.

Figure 6. **Effects of Time Averaging for “Static” and “Dynamic” Tweed:** (a) Instantaneous snapshot of real-space positions. Notice that the tweed easily discerned in the upper sample is obscured by the large thermal fluctuations in the higher temperature (bottom) sample. (b) Average of 30 real-space configurations recorded during simulation. Tweed is visible in the top row, but the deformation has averaged to almost zero in bottom row. (c) Average of 30 diffraction patterns calculated during simulation. Note that instantaneous tweed-like fluctuations are present in *both* cases. Length of simulations: 150,000 attempted Monte Carlo steps (approximately one nanosecond).

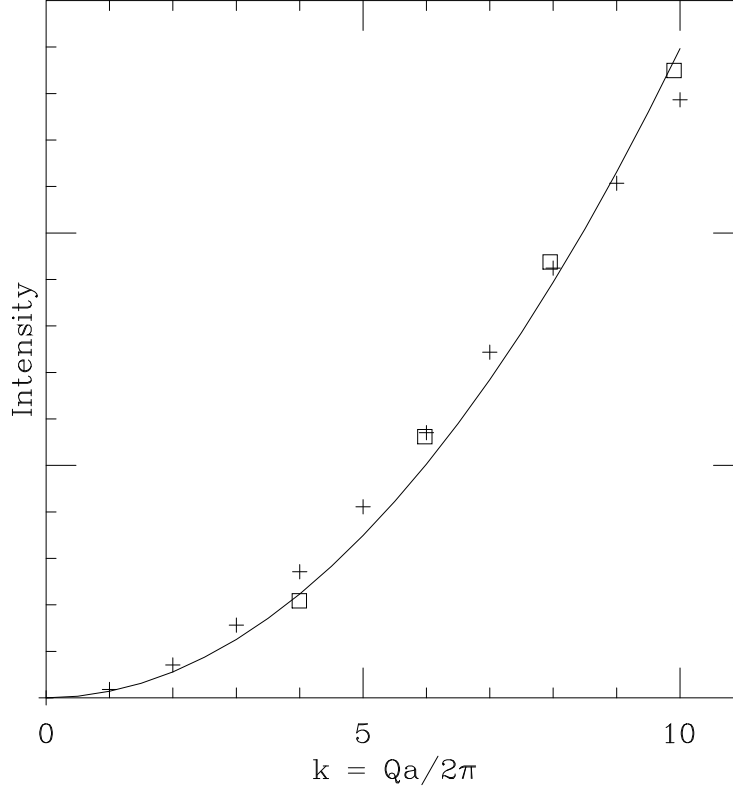


Figure 7. **Diffuse Scattering Intensity vs. Wavevector:** The squares are experimental measurements¹⁴ of diffuse scattering intensity at $\mathbf{Q} = \langle 0 \ Q \ 0 \rangle + \epsilon$ where $Q/(2\pi/a) = 4, 6, 8, 10$ and $\epsilon = \langle .06 \ .06 \ 0 \rangle$. The crosses are simulation data, scaled by a single constant for comparison to the experimental data. The curve is a fit to $I \sim |\mathbf{Q}|^2$, which would be exact in the limit of infinitesimally small displacements.

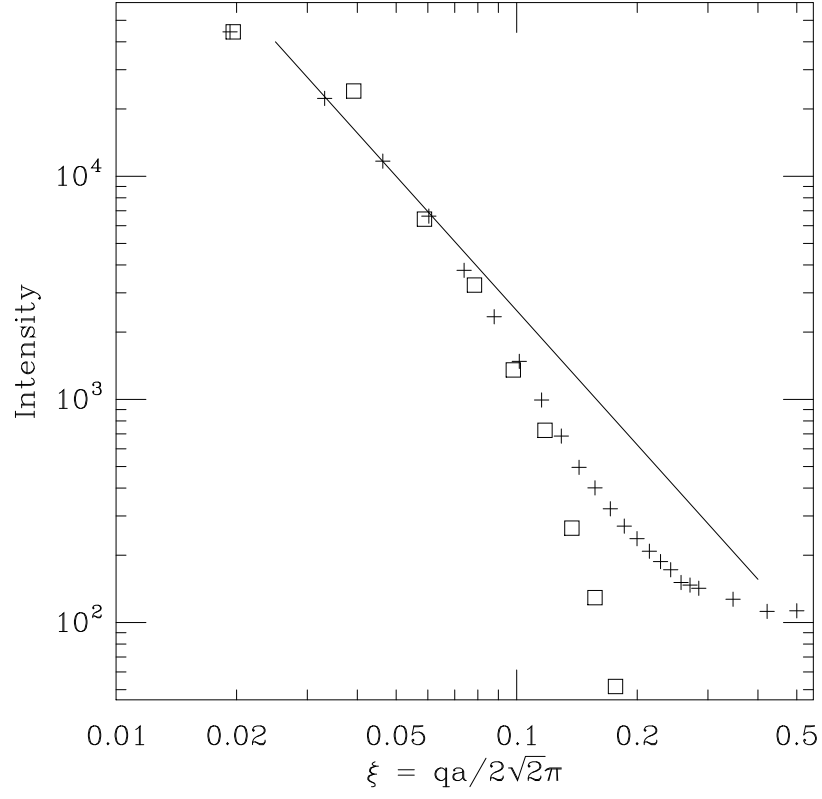


Figure 8. **Intensity of Diffuse Scattering** in the $\langle\bar{1}10\rangle$ direction around Bragg peak $\langle 660\rangle$. The experimental data¹⁴ are shown with crosses, the simulated data with squares. The line is for comparison to a $1/q^2$ dependence.

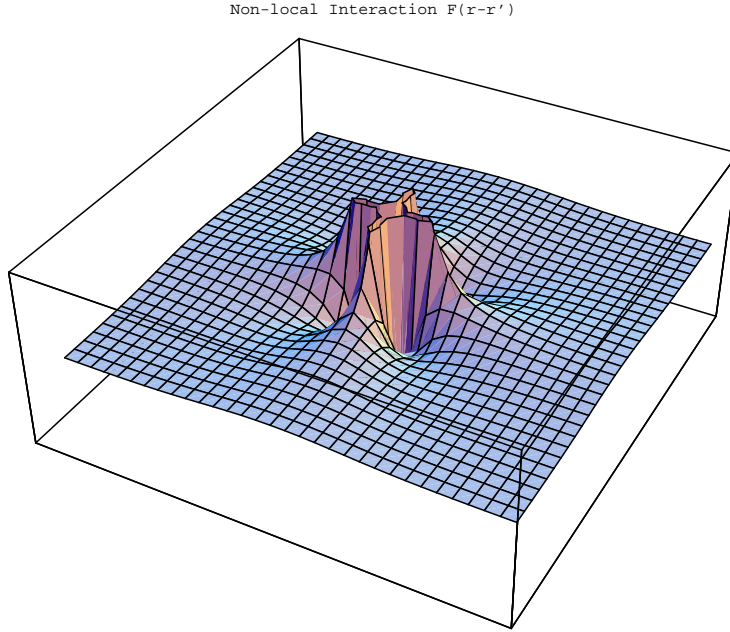


Figure 9. **The long-range nonlocal interaction $f(\mathbf{r}, \mathbf{r}')$.** Summing the two interactions $f_1(\mathbf{r}, \mathbf{r}')$ and $f_2(\mathbf{r}, \mathbf{r}')$, and using materials parameters for FePd as in the simulation, gives us the full form for the nonlocal interaction, $f(\mathbf{r} - \mathbf{r}')$ relating $\phi(\mathbf{r})$ and $\phi(\mathbf{r}')$. (The function is truncated near the origin to maintain a reasonable scale.)

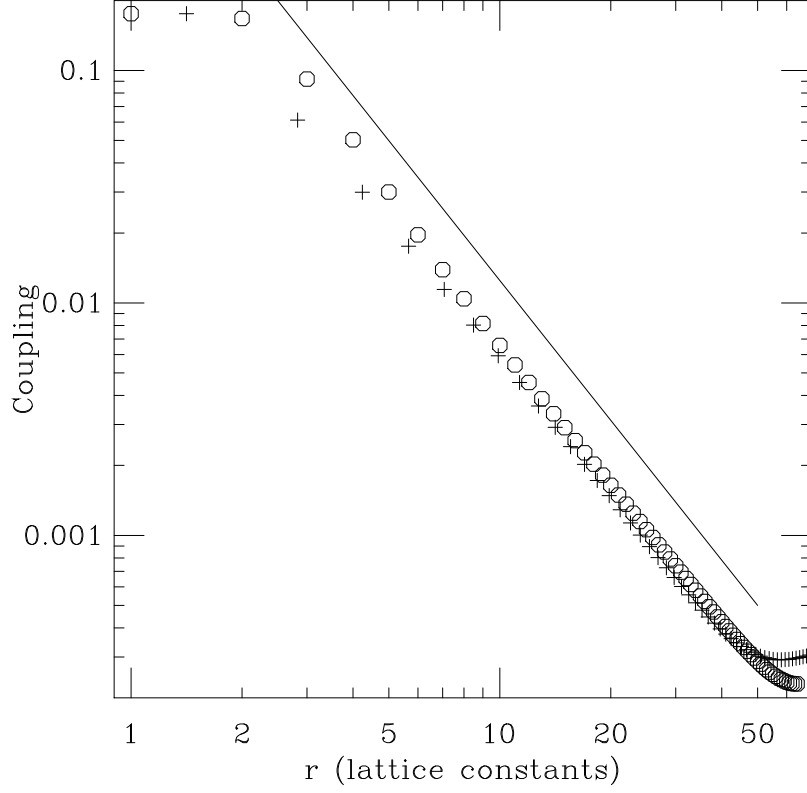


Figure 10. **The long-range nonlocal interaction** is plotted along the diagonal (crosses) and axial (circles) directions. Note the $1/|\mathbf{r}|^2$ dependence of the interaction strength (as indicated by the reference line). Distance is in units of lattice constants, and the y-axis is in arbitrary units. (The tail appearing at long distances is merely an aliasing effect.)

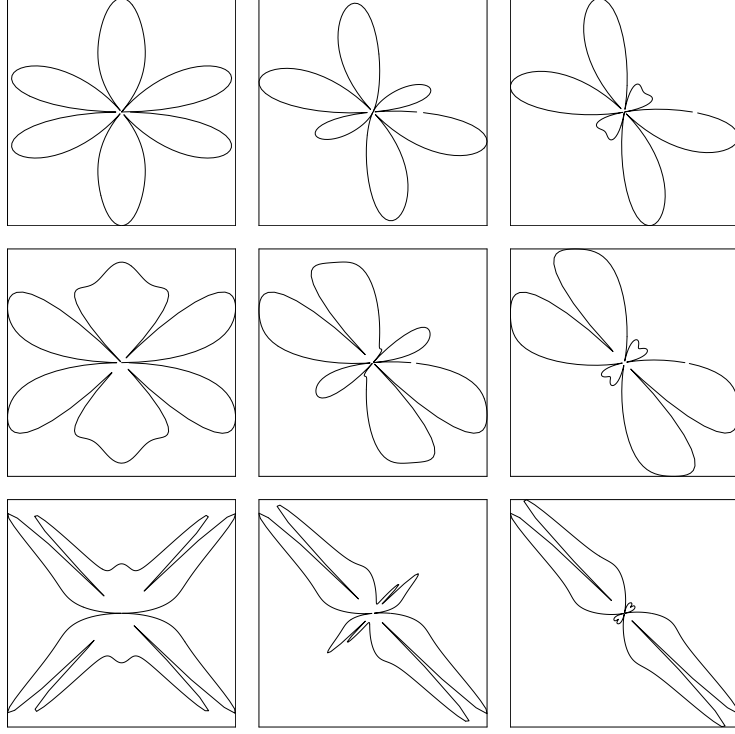


Figure 11. **Diffraction Contours Due to Linear Coupling to e_1 :** Diffraction contour around Bragg peaks $\langle 04 \rangle$, $\langle 24 \rangle$ and $\langle 22 \rangle$ (from left to right) at anisotropies $\alpha = 1$, $\alpha = 5$, and $\alpha = 50$ (from top to bottom.) (The coupling strength D was scaled with the anisotropy, so that the net deformation is constant in magnitude, but increasingly tweedy.) Since tweed can be observed⁹ in FePd, for example, when the anisotropy is as small as $A = 5$, this implies that tweed cannot be explained by a linear response to a coupling to bulk dilation.

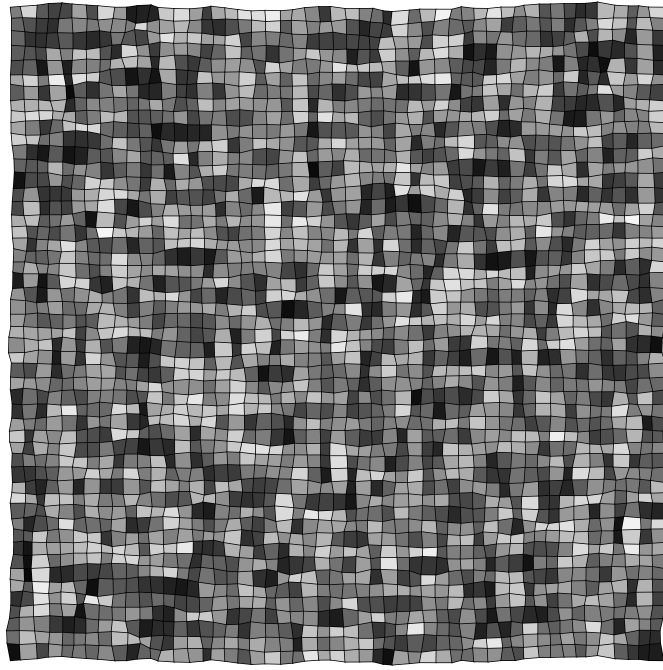


Figure 12. **Configuration resulting from linear coupling to e_1 :** showing substantial deformation, but no identifiably tweedy modulation.